Predicting Radiation-Induced Cell Mutations for Mars Missions: A Microdosimetric Kinetic Model Study

Master's Thesis
University of Turku
Physics
2024
Eeli Kinnunen
Supervised by:
Dr. Andrea Attili
Prof. Maurizio Marrale
Dr. Philipp Oleynik
Examiners:
Prof. Rami Vainio
Dr. Philipp Oleynik

The originality of this thesis has been checked in accordance with the University of Turku quality assurance system using Turnitin Originality Check service.

UNIVERSITY OF TURKU
Department of Physics and Astronomy

Kinnunen, Eeli Predicting Radiation-Induced Cell Mutations for Mars Missions: A Microdosimetric Kinetic Model Study

Master's Thesis, 75 pp.
Physics
November 2024

Ionising radiation from particles caused by solar particle events (SPEs) and galactic cosmic rays (GCRs) poses a cancer risk for astronauts in space. Cell survival and mutation after exposure to ionising radiation can be described with radiobiological models.

This study explores the use of the microdosimetric kinetic model (MKM) in the evaluation of carcinogenic mutations in cells induced by ionising radiation, and the application of the model to a mission on Mars. In addition to using the MKM to evaluate cell survival probabilities, for which it has almost solely been used before, it is used here to evaluate mutation probabilities. Linear quadratic model was used to fit survival and mutation as a function of dose in the experimental data. A subset of available experimental data was used in the identification of the parameters needed in the MKM. Predictions of cell survival and mutation were then carried out by simulations with 'Survival' code utilising the Kiefer-Chatterjee particle track model and compared with the full set of experimental data. Additional analyses accounting for the effect of the dose rate were performed for the datasets that included dose rate information. The results of the simulations resembled experimental data with low linear energy transfer (LET) values more accurately than experimental data with high LET values.

Space radiation conditions on a habitat on Mars were obtained from OLTARIS (On-Line Tool for the Assessment of Radiation in Space). Simulations of cell survival and mutation were carried out for the SPE spectrum using the optimised parameters discovered from the linear quadratic fits and the comparisons to experimental data. Preliminary simulations accounting for the dose rate were currently carried out only for the low doses, in which cases the predictions of cell survival and observable mutation were similar to the predictions of the simulations not accounting for the dose rate.

Predicting the probability of observable cell mutation is the first step in modelling cancer risk. The methods presented in this study could assist in the evaluation of carcinogenic mutations caused by ionising radiation, including the effects of radiation on a space mission.

Keywords: space radiation, microdosimetric kinetic model, cell mutation, space mission, Mars

Contents

1 Introduction

Ionising radiation in near Earth space can be categorised into three groups: particles that are trapped inside the Earth's magnetic field, particles caused by solar particle events (SPEs), and galactic cosmic rays (GCRs) originating from outside the solar system. In SPEs electrons, protons and other nuclei are accelerated during a solar flare or by a shock driven by a coronal mass ejection (CME) (NCRP, 2006). SPEs are sporadic events, lasting from hours to days, ranging in energies from keV to GeV with varying dose rates. For example, dose rates of 1500 mGy/hour have been measured (NCRP, 1988). GCRs consist of a continuous fluence of nuclei likely accelerated by electromagnetic fields of supernova remnants. Their energies vary from 10 MeV/nuc to more than 10 GeV/nuc. Approximately 87 % of them are hydrogen ions, 12 % helium ions and 1–2 % nuclei from lithium to nickel, and rarely even heavier ions (Simpson, 1983). Dose rates vary from 150 to 300 mGy/year at solar minimum and from 50 to 100 mGy/year at solar maximum. The difference is due to the attenuation of the GCRs by the solar wind in the heliosphere. Attenuation increases with the increasing solar wind pressure during solar maximum and decreases during solar minimum. (Chancellor et al., 2021; Rahmanifard et al., 2020)

Space radiation is characterised by high energy and a low dose rate setting it apart from most radiation sources in medical applications. Other characteristics, such as microgravity, create further challenges in assessing carcinogenic effects of radiation exposure of astronauts in space missions (Guo et al., 2022). However, in terms of the types of particles and energy ranges, space radiation has similarities to irradiation used in clinical applications, in particular ion beam radiotherapy. Space radiation is abundant in heavy charged particles with high linear energy transfer (LET). Even though total radiation doses are low, high LET radiation of low dose rate may present a cancer risk for astronauts in space. This includes astronauts on board the International Space Station (ISS), on a journey to Moon or on a journey

to Mars. (Han et al., 1998)

Dose expressed in grays refers to the radiation dose absorbed by the tissue. This is the unit used in the microdosimetric kinetic model (MKM) based evaluation of radiation and in ion beam therapy. Equivalent dose and effective dose, expressed in sieverts (Sv), are important in dosimetry and radiation protection. Equivalent dose is the absorbed dose multiplied by the radiation weighting factor, W_R, reflecting the type and energy of the radiation. In the case of a mixed radiation field, each equivalent dose is summed over all types of radiation to the total equivalent dose. Effective dose is the equivalent dose multiplied with the tissue weighting factor, W_T, of specified tissues and organs in the human body, used to express stochastic health risks including the probability of cancer induction and genetic effects.

This study explores the use of the MKM in the evaluation of carcinogenic mutations in cells induced by ionising radiation, and the application of the model to a mission on Mars. Thus far the main application of the MKM has been clinical, and it has been used to evaluate cell survival. The extension of the model to evaluate mutations presented in this thesis is new. An additional new aspect is extending a model from a clinical use to a space radiation risk analysis. Given the wide interest in space travel and the prospects of missions to Moon and Mars by NASA, ESA, and private spaceflight companies, the topic of this study is both timely and significant. The tools provided for evaluating radiation effects could hopefully eventually assist in the assessment of health risks to astronauts.

2 Cell Survival and Mutation After Exposure to Ionising Radiation

2.1 Theoretical Background

2.1.1 Linear Quadratic Model

Considering probabilities at a population level, if a human population is exposed to ionising radiation with a total dose of $3.5 - 4$ Gy, the total fatality is expected to be 50 % without treatment in 60 days. With treatment and antibiotics, the corresponding threshold dose range is $4.5 - 7$ Gy. Rapid access to various treatments increases the dose range to $7 - 9$ Gy. A total body exposure of 10 Gy or more results in 100 % fatality. (López & Martín, 2011)

Responses to radiation can be described and predicted not only at a population level but also within the organisms at a cellular level. The linear quadratic model (see the next paragraph) is considered the most accurate in describing cell survival after irradiation with ionising radiation in radiobiology and radiotherapy, as it gives the best fit to experimental data. Cell survival refers to a cell maintaining its reproduction ability and cell killing to a loss of that ability. Generally, when the dose is more than 2 Gy, cell killing predominates over cell survival (Prasanna et al., 2014).

The equation of the linear quadratic model that connects cell survival with the irradiated dose is

$$S = \exp(-\alpha D - \beta D^2), \tag{1}$$

where S is the probability of cell survival, α and β are parameters that describe the cell's radiosensitivity, and D is the irradiation dose. Figure 1 shows an example illustration of linear quadratic survival curves. (McMahon, 2018)

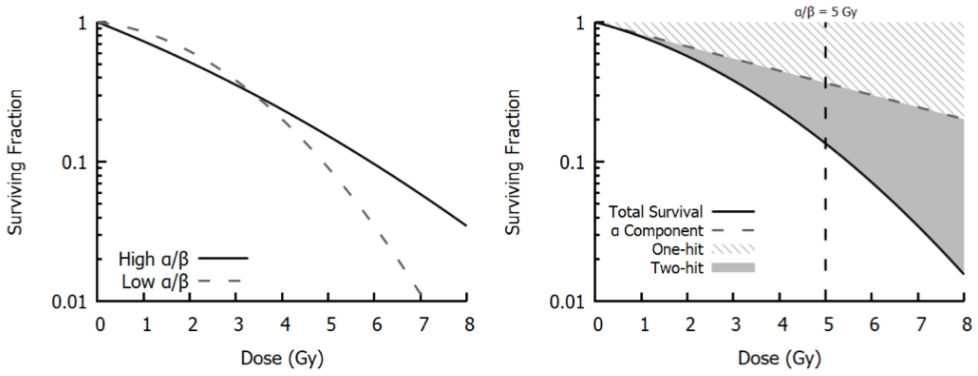

Figure 1. Linear quadratic curves taken from McMahon (2018). One-hit refers to events, where energy deposition from a single incident particle track causes lethal damage to the cell. Two-hit refers to events, where energy deposition from different particle tracks causes interacting damage leading to the death of the cell.

Instead of killing the cell completely, irradiation can damage the sensitive part of the cell containing the genetic information of the cell, namely the DNA in the nucleus. Most DNA damages are repaired by the cell. However, non-repairable damages can lead to mutations in the DNA that can produce neoplastic cell transformations, where cells divide rapidly, which in turn can lead to the formation of tumours in the tissue (Borek et al., 1978; Reznikoff et al., 1973).

Linear quadratic behaviour has also been experimentally observed in mutation curves as a function of dose. Probability of no mutation with the irradiated dose can be expressed as

$$\mu(D) = \exp(-(\alpha_0' D + \beta_0' D^2)) \tag{2}$$

The probability of mutation is then the complement

$$M = 1 - \mu(D) = 1 - \exp(-(\alpha_0' D + \beta_0' D^2)) \tag{3}$$

Observable mutations and observable mutations per surviving cells are two different values. As the irradiation dose increases, more and more cells are killed and therefore unable to mutate. This means the number of observable mutations goes down as the number of killed cells increases, reaching zero when all the cells are

killed. The number of observable mutations per surviving cells, on the other hand, keeps increasing with the dose. In a visual representation shown in figure 2, the curve for observable mutations as a function of dose is below the curve for observable mutations per surviving cells. The probability of observable mutation is the relevant probability when evaluating the carcinogenic radiation risk of the astronaut to estimate how many cells mutate. It is the average of the product of the probabilities of mutation and survival,

$$P = \langle M_c S_c \rangle_c, \tag{4}$$

where S_c is the survival of each one cell in the population of cells, M_c is the mutation of each one cell in the population of cells, and $\langle ... \rangle_c$ is the average over a population of cells. Within this notation, S and M correspond to $\langle S_c \rangle_c$ and $\langle M_c \rangle_c$ respectively. The probability of observable mutations per survivor describes the number of cells that have mutated normalised with the number of cells that have survived observed in experimental data:

$$\tilde{M} = \frac{P}{S} \tag{5}$$

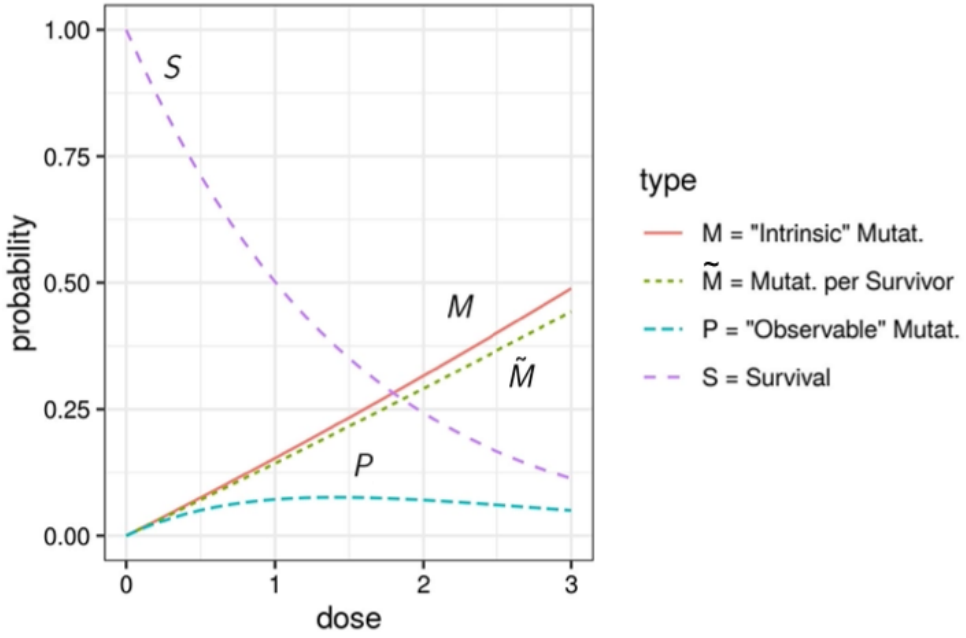

Figure 2. Probability of survival S, probability of mutation M, probability of observable mutation P and probability of observable mutation per survivor $\tilde{M}$.

2.1.2 Microdosimetric Kinetic Model

The process of cell survival and cell transformation after irradiation with ionising radiation can be described with different radiobiological models. These models are used for planning radiation therapy for cancer patients. The MKM along with some other models such as the local effect model (LEM) is based on macroscopic experimental observations, whereas some other models describe the process by detailing the chain of the physical and biological events. The advantages of the models using the first approach are their simplicity and adjustability; the parameters of the models can be adjusted based on experimental data. MKM and LEM are clinically the most widely used in hadron therapy, where irradiation is done with charged nuclei, e.g. protons and carbon nuclei. In general, they have almost solely been used to evaluate cell survival (Manganaro et al., 2018), although there has been at least one attempt to evaluate mutation with the MKM by Attili et al. (2022). In this thesis,

the MKM is used to derive a model that evaluates mutation probabilities in addition to survival probabilities.

The microdosimetric kinetic model is "kinetic" because the cell injuries and repairs – the temporal process of damages to the DNA in the cell nucleus – are described with kinetic equations; and "microdosimetric" because the deposition of energy from irradiated particles is considered from a microscopic – cellular or subcellular – volume (Hawkins, 1996; Hawkins, 1994). Specifically, the cell nucleus as the sensitive target of ionising radiation is divided into subnuclear structures called domains. Within the radius of the domain there can be damaging energy deposition from the combined effect of more than one particle hitting the cell. (Manganaro et al., 2018).

The kinetic equations in the MKM are

$$\dot{x}_I^{(cd)} = \lambda \dot{z}^{(cd)} + a x_{II}^{(cd)} + b (x_{II}^{cd})^2 \tag{6}$$

$$\dot{x}_{II}^{(cd)} = k \dot{z}^{(cd)} - (a+r) x_{II}^{(cd)} - 2b (x_{II}^{cd})^2 \approx k \dot{z}^{(cd)} - (a+r) x_{II}^{(cd)}, \tag{7}$$

where c is the cell, d is a specific domain in the cell, z is the microscopical dose absorbed by the domain, $\dot{z}$ is the dose rate, x_I are type I lesions, i.e., lesions associated with clustered DNA damages that are not repairable and are directly lethal to the cell, and x_{II} are type II lesions, i.e., lesions associated with repairable damages to the cell. $\dot{x_I}$ and $\dot{x_{II}}$ are the rates of production of the respective lesion types, and λ and k are their proportionality constants to the dose rate. a is the first-order rate constant for spontaneous formation of a lethal lesion from a type II lesion that spontaneously converts to an irreparable lesion, b the second-order rate constant for the formation of a lethal lesion from a pair of type II lesions, and r the first-order repair constant for the repair of a type II lesion. The quadratic term $2b(x_{II}^{cd})^2$ is considered negligible compared to the first-order terms in the rate of production of type II lesions. This is because repairs of potentially lethal lesions $(a+r)$ are more common than the formation of lethal lesions from pairwise combinations (b), so the

absolute value of the quadratic term is small compared to the absolute value of the second term. (Attili et al., 2022; Hawkins, 1996; Hawkins, 1998; Manganaro et al., 2017)

When the sequences of doses and times for each domain in each cell are known, the solution to the kinetic equations gives the final amount of type I lethal lesions defined in Manganaro et al. (2017) as

$$\begin{aligned}\tilde{x}_I^{(cd)} = &\frac{\alpha_0}{N_D}\sum_{i=0}^{n_c-1} z_i^{(cd)} + \frac{\beta_0}{N_D}\left(\sum_{i=0}^{n_c-1} z_i^{cd}\right)^2 \\ &- 2\frac{\beta_0}{N_D}\sum_{i=0}^{n_c-2}\sum_{j=i+1}^{n_c-1}\left(1-\exp\left(-\frac{1}{\tau}(t_j^{(c)}-t_i^{(c)})\right)\right) z_i^{(cd)} z_j^{(cd)},\end{aligned} \tag{8}$$

where N_D is the total number of domains constituting the cell nucleus, n_c is a Poissonian random variable that indicates the number of particles that interact with the cell c and the domain d, $\frac{1}{\tau} = (a + r)$ is the time constant that defines the repair kinetics, and α_0 and β_0 represent the acute local effect. The indices i and j refer to the interaction of i^{th} and j^{th} particle. A similar expression is derived also for the lesion $\tilde{x}'_I$ associated to the onset of mutation, with different parameters α'_0 and β'_0. In this case $\tilde{x}'_I$ are not irreparable lethal lesions but irreparable lesions that cause a mutation. (Manganaro et al., 2017)

The probability of survival S and the probability of no mutation μ are expressed in the following manner:

$$S(D) = \langle \exp(-\sum_d x_I^{(cd)})\rangle_c \tag{9}$$

$$\mu(D) = \langle \exp(-\sum_d x\prime_I^{(cd)})\rangle_c \tag{10}$$

In the limit of low LET they can be approximated as

$$S(D) \approx \exp(-(\alpha_0 + \beta_0 z_{1d})D - \beta_0 D^2) \tag{11}$$

$$\mu(D) \approx \exp(-(\alpha'_0 + \beta'_0 z_{1d})D - \beta'_0 D^2), \tag{12}$$

where α_0 is associated to the linear quadratic parameter α when LET approaches 0, and β_0 to the linear quadratic parameter β when LET approaches 0. D is the macroscopic dose and z_{1d} is the dose-mean specific energy absorbed by the cell domains in a single event. (Attili et al., 2022; Hawkins, 1998, 2003)

The relative biological effectiveness (RBE) refers to the ratio of the biological effect of ionising radiation to X-ray radiation, when the amount of absorbed energy is the same. The biological effect considered is typically cell survival. The dependence of RBE on LET has been experimentally observed; RBE at first increases with increasing LET, and then decreases at higher LET. RBE maximum is in the approximate range of LET $50 - 200$ keV/μm. In the MKM this dependence is explained by the energy deposited in the microscopic regions in the cell nucleus and random variations of this energy. (Hawkins, 1998)

2.1.3 Particle Track Model

When the ions hit the cell nucleus, they deposit energy. The microscopic energy deposition is a stochastic process, and each cell has a different pattern of energy deposition. The description of this deposition of each ion along the particle tracks can be modelled with an amorphous-track approach. The Kiefer-Chatterjee model describes the core and the penumbra of the track by combining two models: the Chatterjee model (Chatterjee & Schaefer, 1976) describes the track structure within the core radius and the Kiefer model (Kiefer & Straaten, 1986) within the penumbra region, which is the external part of the track. The track is not present beyond the penumbra radius indicating a zero dose of radiation. Average radial dose distribution around the trajectory of the ion is assumed for amorphous track models, including the Kiefer-Chatterjee model. The core radius, R_c, and penumbra radius, R_p are

calculated in the following manner:

$$R_c = 0.0116\beta_{\text{ion}}\ [\mu\text{m}] \tag{13}$$

$$R_p = 0.0616\left(\frac{E}{A}\right)^2\ [\mu\text{m}], \tag{14}$$

where E is the energy in MeV, A is the mass of the ion in atomic mass units and β_{ion} is the ion velocity relative to the speed of light. The penumbra dose, D_p, as a function of track radius r in units of μm, is calculated in the following manner:

$$D_p(r) = 1.25 \cdot 10^{-4}\left(\frac{z^*}{\beta_{\text{ion}}}\right)^2 r^{-2} \equiv K_p r^{-2}\ [\text{Gy}], \tag{15}$$

where z^* is the effective charge in the Barkas expression. The previous formula also defines the parameter K_p used in the calculation of the constant core dose D_c:

$$D_c = \frac{1}{\pi R_c^2}\left(\frac{LET_\infty}{\rho} - 2\pi K_p \ln\left(\frac{R_p}{R_c}\right)\right)\ [\text{Gy}], \tag{16}$$

where LET_∞ is the unrestricted linear energy transfer of the incident ion in keV/μm and ρ is the mass density of water in g/cm^3. (Elsässer et al., 2008; Kase et al., 2008)

2.1.4 Survival and Mutation Simulations

Theoretical predictions of cell survival and mutation after irradiation with different ions was done in 'Survival' code developed at the INFN (Istituto Nazionale di Fisica Nucleare) in collaboration with the University of Torino (UniTO, Physics Department). The MKM with the Kiefer-Chatterjee model of the particle track structure is implemented in the code. 'Survival' was initially developed for a clinical application, for the purpose of radiobiological computations needed in ion beam therapy to aid in the planning of treatments for cancer patients (Manganaro et al., 2018).

The ion types, either their energies or LETs, and the doses delivered are needed as input for the description of the radiation spectrum in 'Survival'. The four parameters of the MKM are also needed: α_0, β_0, the radius of the cell nucleus r_N, and the radius of the domain r_D. For the mutation induction modelling a Monte Carlo

time dependent approach is used to track the amount and time of energy deposition within each domain within each cell nucleus. Each domain is given its own specific random sequence and random time interval of deposition of energy. (Manganaro et al., 2018)

To verify whether ion isotopes, namely deuterium and helium-3, could be included to the analysis with 'Survival' code, the Kiefer-Chatterjee amorphous track model and the Bethe-Bloch formula were analysed. The 'Survival' code obtains the kinetic energies of the ions from the LETs of the ions, or vice versa the LETs from the energies, by applying a simulation of the Bethe-Bloch formula that describes the stopping power of the material. The Bethe-Bloch formula within the code is simulated with SRIM software that evaluates the stopping power of each ion as a function of specific energy (energy per nucleon). The LET is approximated with this stopping power. The linear electronic stopping power is identical to the unrestricted linear energy transfer used in the Kiefer-Chatterjee model present in equation (16) for the core dose. In addition, the model accounts for specific energy instead of absolute energy, as shown in equation (14) for the penumbra radius, and for the charge in equation (15) for the penumbra dose. Even though the absolute energy is different between hydrogen and deuterium, as well as between helium-4 and helium-3, the specific energy and the charge are the same, so the results could be obtained for all the isotopes.

2.2 Methodology

2.2.1 Overview of the Methods

The general idea of the analysis was to use a subset of the available experimental data for identification of the parameters needed in the MKM. These parameters were then used to predict cell survival and mutation with 'Survival'. This prediction was compared with the full set of the experimental data to validate or invalidate the

MKM used in 'Survival'.

Existing experimental publications were surveyed to find the ones relevant for space radiation studies and suited for the procedure of testing the mutation model derived from the MKM. Suitable studies needed to include data for both cell survival and neoplastic cell transformation. In other words, one biological endpoint of the study had to be cell survival (how many cells survived the irradiation) and the other endpoint cell transformation (how many cells showed signs of neoplastic transformation after irradiation). Cell mutation is rare compared to cell killing, so such data are scarce due to large amounts of cells needed to obtain significant results. The studies also needed to include data from low LET particles, such as gamma or X-ray irradiation, for the determination of the parameters in the model. In addition, at least some of the data had to be from irradiation with ions between hydrogen and neon in the periodic table. 'Survival' code currently supports ions from hydrogen to neon, and the present implementation does not include data of the stopping power vs. energy for heavier particles. The track model itself can be applied beyond neon, so such data could be added later to extend the application to heavier particles. Four published studies fulfilled these criteria. The *in vitro* data of cells irradiated with ion beams were collected from these publications: Han et al. (1998), Miller et al. (1995), Yang et al. (1996), and Yang et al. (1985). Survival and mutation curves of the studies representing the cell response to different radiation doses were manually digitised with WebPlotDigitizer (Rohatgi, 2022).

First, the linear quadratic model was used to fit survival as a function of dose in the experimental data. The values for the parameters α and β were given by the fit. Second, a subset of the values derived for α and β as a function of LET and particle were then used to derive the MKM parameter values for α_0 and β_0 for the datasets in each publication. Low LET particles of less than 50 keV/μm were chosen as the subset. Two approaches were tested in this step: extrapolating α_0 and

β_0 at LET = 0 from low LET particles such as photons, and estimating α_0 and β_0 as an average of low LET particles. The approaches are described in detail when they are applied. It should be noted here that α and β values depend not only on the LET of the particle but also on the charge and the mass of the particle. However, the difference in the α and β values between particles with different charge and mass is generally small compared to the difference between particles with different LETs (Furusawa et al., 2000). Therefore, especially when the datasets are small, different types of particles with similar LETs can be grouped together to determine the general trend of the α and β values.

Finally, the values derived for α_0 and β_0 were used to evaluate the two other parameters, r_N and r_D, also needed in the MKM. This evaluation was done by finding such values of r_N and r_D that minimised the difference between the experimental data and the output from the MKM simulation in 'Survival'. A range of values for r_N and r_D were chosen, and the combination of the two that minimised the difference was chosen as the optimal one. An alternative approach of choosing a range of values for all four parameters, α_0, β_0, r_N and r_D, was also tested. The combination of all four that in the simulation produced the closest resemblance of experimental data was chosen as the optimal one.

The same process was then repeated for modelling mutation as a function of dose with one exception: in the final step $r_N^{'}$ was assumed to be the same as when modelling survival, and only a suitable value for $r_D^{'}$ was tested. Analytical approximation of $S(D) = \langle \exp(-\sum_d x_I^{(cd)}) \rangle_c$ derived by Hawkins (2003) was used for the survival data in 'Survival'. This is referred to as 'rapid calculus'. Monte Carlo approach was used to evaluate both $\langle \exp(-\sum_d x_I^{(cd)}) \rangle_c$ and $\langle \exp(-\sum_d x\prime_I^{(cd)}) \rangle_c$ as described by Manganaro et al. (2017) and Attili et al. (2022) for the mutation data.

Python programming language was used in all data analysis. Simulations written in C++ in 'Survival' were run as subprocesses in Python. Computationally heavy

Monte Carlo simulations were carried out in the computer cluster Dione of the University of Turku.

2.2.2 Experimental Data

In the *in vitro* experiment in the first study by Han et al. (1998), Syrian hamster embryo cells (cell line SHE) were irradiated with X-rays and carbon ion beams. Cell colonies that were morphologically altered were classified as transformants. In all the other experiments by Miller et al. (1995), Yang et al. (1985), and Yang et al. (1996), mouse embryonic stem cells (cell line C3H10T1/2) were irradiated. Oncogenic transformation of cells was determined after irradiation. In this thesis the transformants in all the datasets are referred to as mutations. Relevant radiation types were X-rays, carbon, and neon ion beams from the second study; X-rays, deuterium, hydrogen, helium-3, helium-4, carbon, oxygen, and fluorine ion beams from the third study; and gamma rays and neon ion beams from the fourth study.

Low LET radiation (e.g. X-ray and gamma ray) experiments are used as a reference to high LET heavy-ion experiments. In the Yang et al. (1985) dataset the heavy-ion measurements were done on different days. Therefore, the experiment with the reference X-ray radiation was repeated on the same day of the heavy-ion measurements due to possible changes in the measurement conditions. In the figures throughout this study the two different X-ray measurements in the Yang et al. (1985) dataset are identified by adding the heavy element in parenthesis: X-rays (C) and X-rays (Ne). The ions and their LET values are listed in table I. Ions were accelerated to different energies.

Two datasets included information about dose rate. In the Han et al. (1998) dataset the dose rates were $0.04 - 0.20$ Gy/min for low dose irradiation and $1 - 2$ Gy/min for high dose irradiation with carbon beams. In the absence of information about specific dose rates with each dose, an average of 0.12 Gy/min was assumed

for doses up to 1 Gy and 1.5 Gy/min for higher doses in the subsequent analysis. The Yang et al. (1996) dataset specified two different dose rates, 0.02 Gy/min and 2 Gy/min, for neon ion beams with the same LET.

Each experimental dataset was analysed separately to determine the best parameters for each dataset needed in the MKM.

Table I. Ions and their LET values in the four experimental datasets.

Han et al. (1998)		Miller et al. (1995)		Yang et al. (1985)		Yang et al. (1996)	
Ion	LET [keV/μm]	Ion	LET [keV/μm]	Ion	LET [keV/μm]	Ion	LET [keV/μm]
C	13	D	3.8	C	10	Ne	32
C	50	D	40	Ne	32		
C	100	H	15				
		^{3}He	75				
		^{4}He	90				
		^{4}He	120				
		^{4}He	150				
		^{4}He	200				
		C	265				
		O	418				
		F	600				

2.2.3 Linear Quadratic Fits

Scientific computation library SciPy in Python and its optimisation package were used to fit a function based on the linear quadratic model to the experimental survival and mutation data. The fitting function based on the linear quadratic model

giving the probability of cell survival after irradiation was

$$S = \exp(-\alpha_S \cdot D - \beta_S \cdot D^2), \tag{17}$$

where S is the probability of cell survival after irradiation, D is the irradiation dose, and α_S and β_S are the parameters to be fitted.

The fitting function giving the probability of cell mutation after irradiation was

$$M = 1 - \exp(-\alpha_M \cdot D - \beta_M \cdot D^2), \tag{18}$$

where α_M and β_M are the parameters to be fitted. In some cases, the experimental data revealed a small mutation probability for zero doses of irradiation. These are spontaneous mutations not related to irradiation. Therefore, an offset value was calculated and the data corrected accordingly to begin from no mutations for zero dose.

An example of the linear quadratic fits of the survival data is shown in figure 3. The figure includes simple fits indicated with a solid line and the mean of fits utilising bootstrapping (random sampling with replacement) indicated with a dashed line. In this and all the successive figures the shaded regions represent the limits of 10 % and 90 % percentiles of the full distribution obtained from bootstrapping. With bootstrapping, re-sampled datasets were created from the original experimental data points. The size of each re-sampled dataset is the same as that of the original dataset. The data points are selected at random, with each data point having the same probability for selection. The same data points can get chosen several times, whereas some data points might not get chosen even once. The benefit of bootstrapping is that it accounts for fluctuations and uncertainty in the data. These fluctuations and uncertainties are present in the experimental data of the four studies, however, with bootstrapping their effect on the results is accounted for. Since the mean values derived from the bootstrap distribution of fits mostly converged with the direct simple fits, only the bootstrap fits were used in the subsequent analysis.

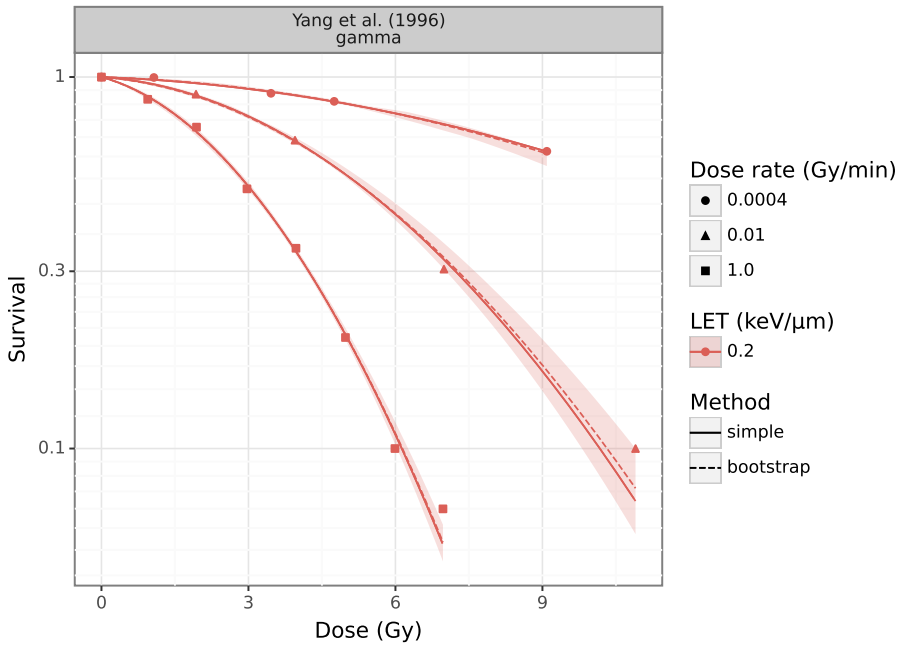

Figure 3. An example of linear quadratic fits of the experimental *in vitro* survival data.

Initially, different datasets of bootstrap replica samples were created. A heuristic approach was used to determine the number of replica samples, starting from 10000, which was assumed to be enough for statistical convergence. Within that dataset, smaller datasets of 100, 1000, 2000, 3000, 4000 and 5000 replica samples (chosen at random) were created. As the comparisons for mean α_S and mean β_S in figures 35 and 36 in Appendix show, the statistics are similar in all the re-sampled datasets, especially for greater than 1000 replica samples. To err on the side of caution, a dataset of 2000 replica samples was used in all the subsequent analysis utilising bootstrapping. Examples of the distribution of cell survival and mutation with the bootstrap method are shown in figures 37 and 38 in Appendix.

2.2.4 α_0 and β_0 Parameters

In the MKM, parameters α_0 and β_0 are the values of α and β, when the LET of a particle approaches 0 keV/μm (see equation (11)). The same applies for the

mutation parameters α_0' and β_0' (see equation (12)). Typically, they are directly extracted from the α and β of experimental measurements of X-ray or gamma ray data as approximations of α_0 and β_0, as both have low LET values. This approach was tested. However, when proceeding with the analysis and choosing them as the α_0 and β_0 parameters in the MKM and comparing the experimentally observed survival and the survival predicted by the MKM (described in chapter 2.3), the survival predicted by the MKM was not consistent with the experimentally observed survival. Therefore, this approach was discarded. To increase the accuracy of the MKM prediction when compared to the experimental data, two other approaches to evaluate α_0 and β_0 were tested: extrapolation from the low LET particles of the experimental data with a linear fit, and estimation as an average of the low LET particles. Particles with LET under 50 keV/μm were included in the extrapolation and averaging.

2.2.5 Dose Rate Analysis

Additional analyses accounting for the dose rate were performed for the two datasets that included information about the dose rate, namely the Han et al. (1998) and the Yang et al. (1996) datasets. A modified version of the 'Survival' code was used in the MKM simulations accounting for the dose rate.

The quadratic part of the linear quadratic fitting function was modified with Lea-Catcheside factor G to account for the dose rate (Brenner et al., 1998). The factor G is the autoconvolution of the dose rate as a function of time $\dot{D}(t)$

$$G = \frac{2}{D^2} \int_{-\infty}^{+\infty} \dot{D}(t)dt \int_{-\infty}^{t} \exp(-(t-t')/\tau)\dot{D}(t')dt', \tag{19}$$

where τ is a time constant to be fitted (the same τ as in equation (8)).

The new fitting function giving the probability of cell survival after irradiation is now

$$S = \exp(-\alpha_S \cdot D - G \cdot \beta_S \cdot D^2), \tag{20}$$

where S is the probability of cell survival after irradiation, α_S and β_S are the parameters to be fitted, and D is the irradiation dose. In this case, assuming a constant dose rate during the cell irradiation, the factor G is defined as

$$G = \frac{2\left(\frac{T}{\tau} - 1 + \exp\left(-\frac{T}{\tau}\right)\right)}{\left(\frac{T}{\tau}\right)^2}, \tag{21}$$

where

$$T = \frac{D}{\dot{D}}. \tag{22}$$

In a single energy deposition event, the number of lesions doesn't depend on τ. In a sequence of energy deposition events, however, the total number of lesions depends on τ and the time intervals between two particle events. Based on equation (20), a higher dependence on the dose rate is expected when considering high doses, and vice versa a lower dependence when considering low doses. The corresponding fitting function giving the cell mutation after irradiation is now

$$M = 1 - \exp(-\alpha_M \cdot D - G \cdot \beta_M \cdot D^2). \tag{23}$$

Since there are two different correlated kinetic processes in mutation – unlike in survival, where there is only one – it is uncertain whether this formula holds in general. However, based on a mathematical consideration it should hold at least for LET approaching 0 keV/μm. In addition, when LET approaches 0 keV/μm, the time constant $\frac{1}{\tau}$ is very similar both for survival and mutation.

As before, two methods were tested to determine the parameters α_0 and β_0: extrapolation from the low LET particles of the experimental data with a linear fit, when the LET of a particle approaches 0 keV/μm; and estimation as an average of the low LET particles. Same approach was tested with the new τ parameter needed to account for the dose rate.

2.3 Results

2.3.1 Results of the Linear Quadratic Fits

Linear quadratic fits of the survival data grouped by publication and particle are shown in figure 4.

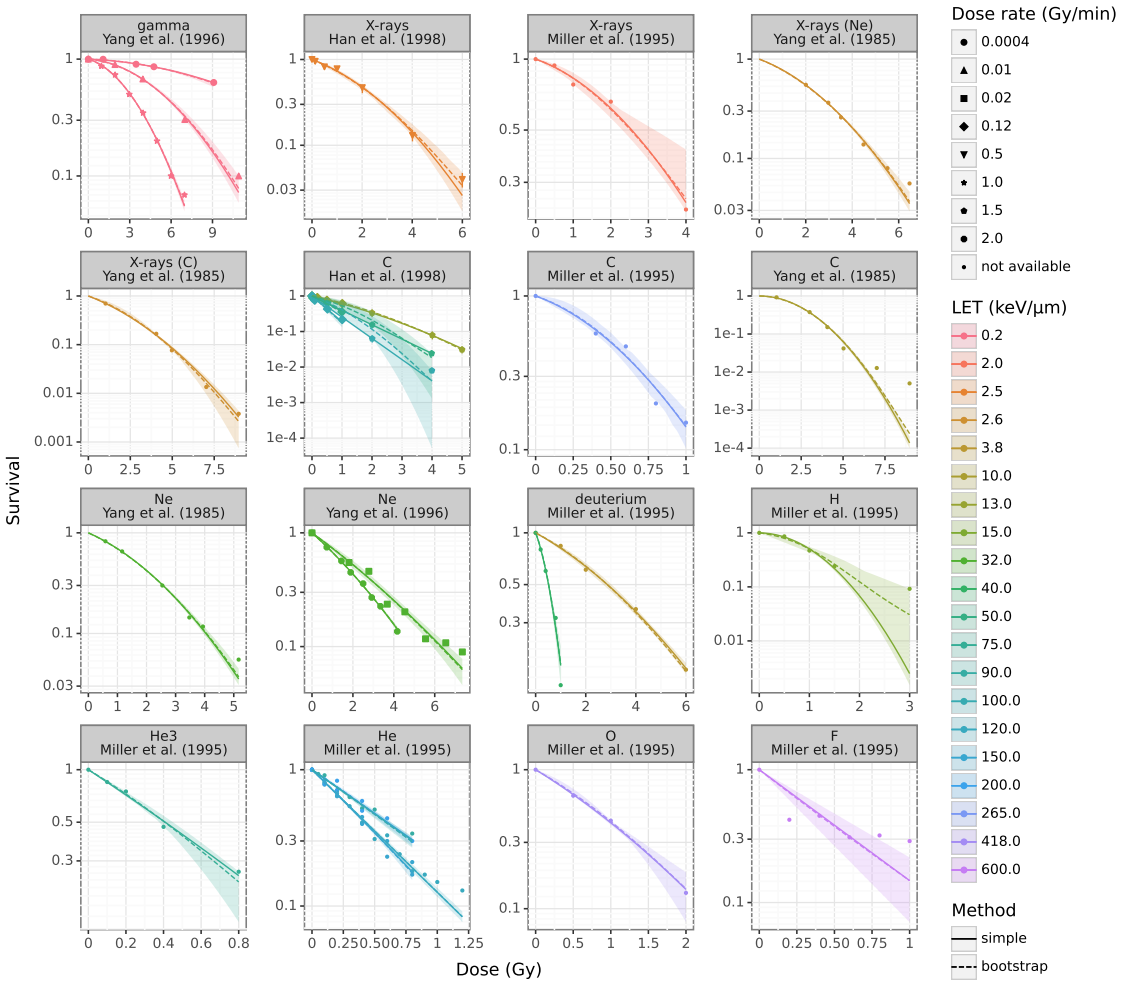

Figure 4. Linear quadratic fits of the experimental *in vitro* survival data.

Similarly, linear quadratic fits of the mutation data grouped by publication and particle are shown in figure 5.

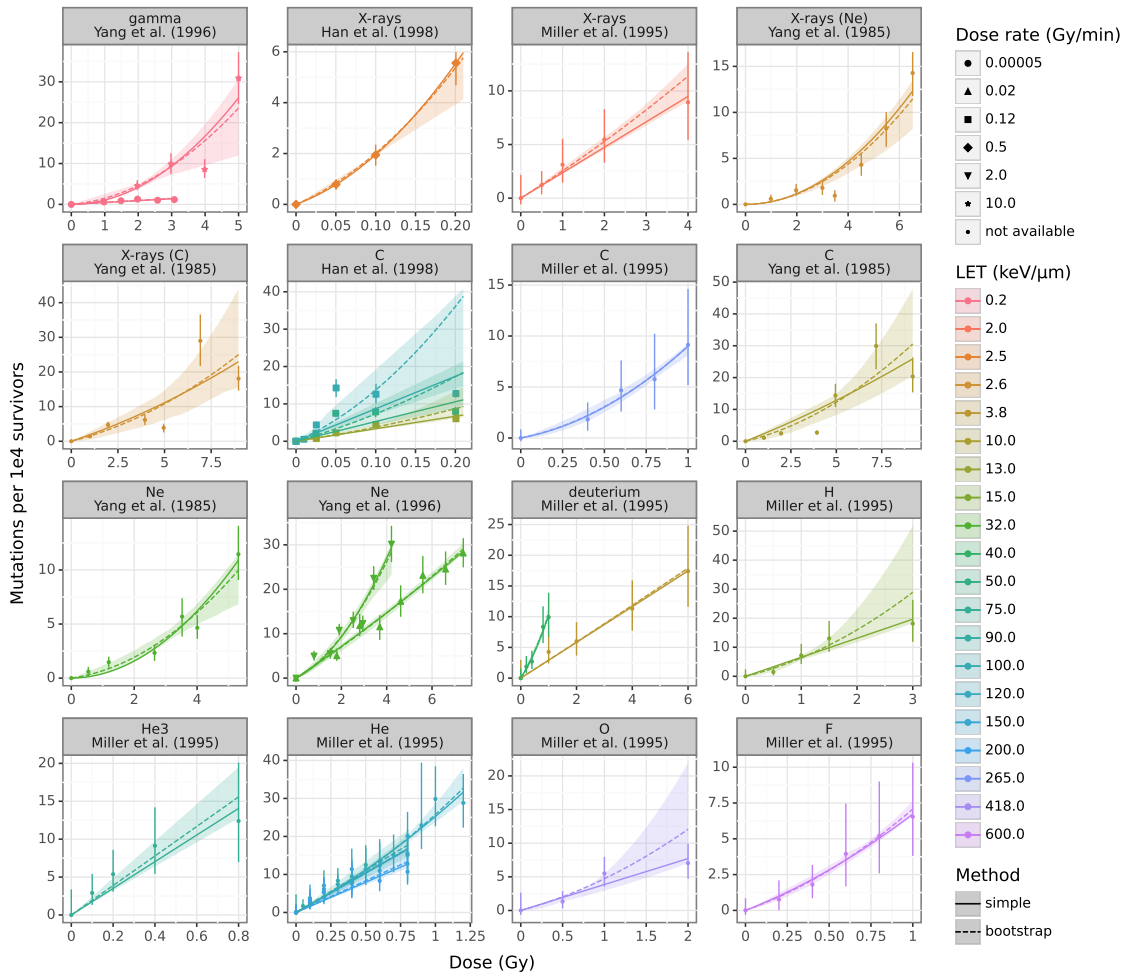

Figure 5. Linear quadratic fits of the experimental *in vitro* mutation data.

From these fits the values of α and β parameters of the linear quadratic model were collected for each particle with a particular LET. The values of α parameter in experimental survival and mutation data vs. LET grouped by publication are shown in figures 6 and 7. The values of β parameter in experimental survival and mutation data vs. LET are shown in figures 39 and 40 in Appendix.

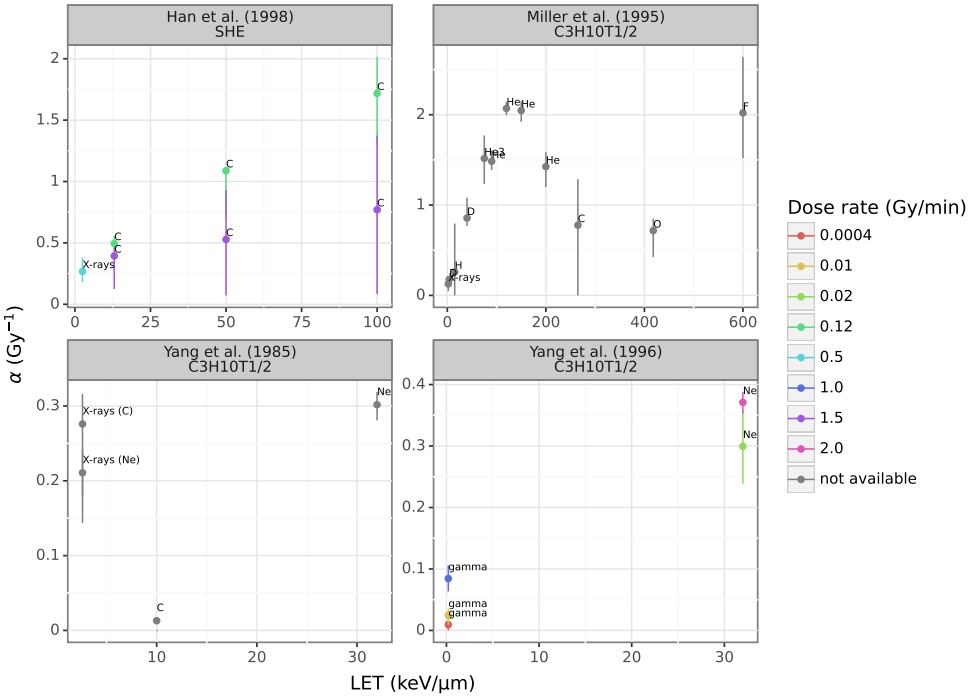

Figure 6. Experimental α vs. LET from survival data.

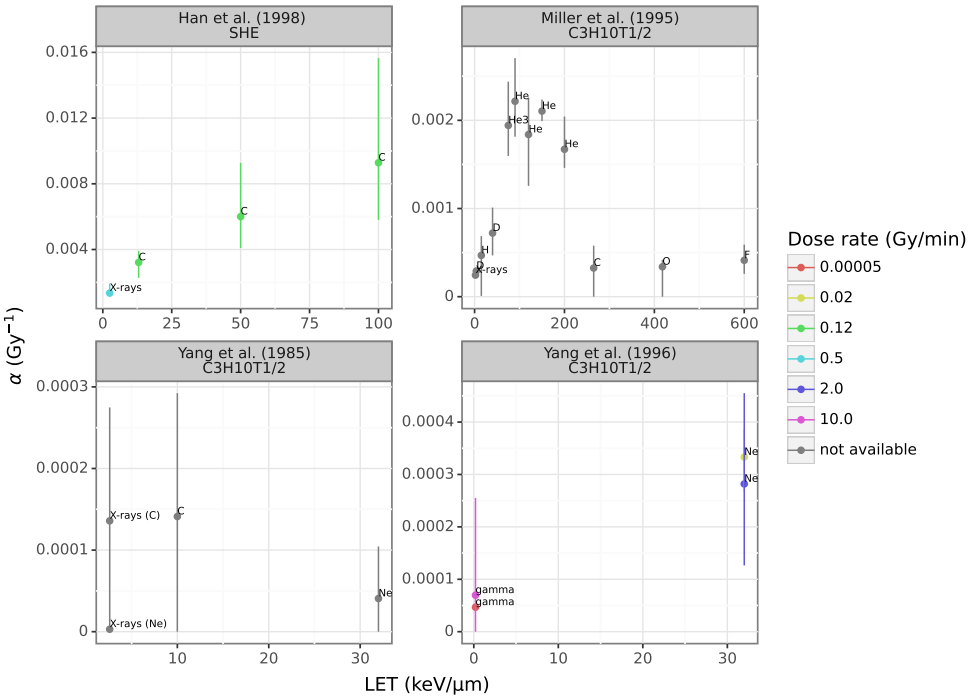

Figure 7. Experimental α vs. LET from mutation data.

2.3.2 Results of the α_0 and β_0 Parameters

Figure 8 shows the results of both approaches, extrapolation and averaging, for finding the α_0 values in each survival dataset. Corresponding results for β_0 values are shown in figure 41 in Appendix. The shaded regions represent the limits of 10 % and 90 % percentiles of the full distribution of α and β obtained from bootstrapping. The results for finding the α_0 values in each mutation dataset are shown in figure 9 and the corresponding results for β_0 in figure 42 in Appendix. As noted, although α and β values depend mostly on the LET of the particle, the charge and the mass of the particle also have an effect. This explains the differences in the α and β values of different particles with similar LETs.

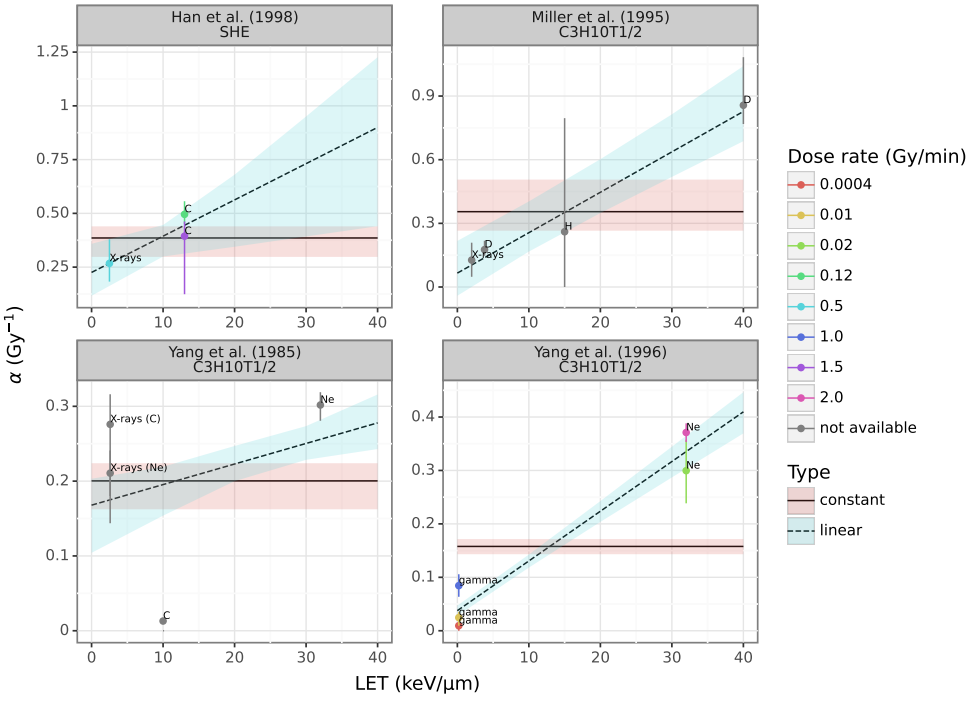

Figure 8. Linear fit of the mean of the bootstrap α as a function of LET in survival data is shown with a dashed line, covering the simple linear fit line. An average value of the mean of bootstrap α is shown with a solid line. Dose rates, when available, are indicated with colours.

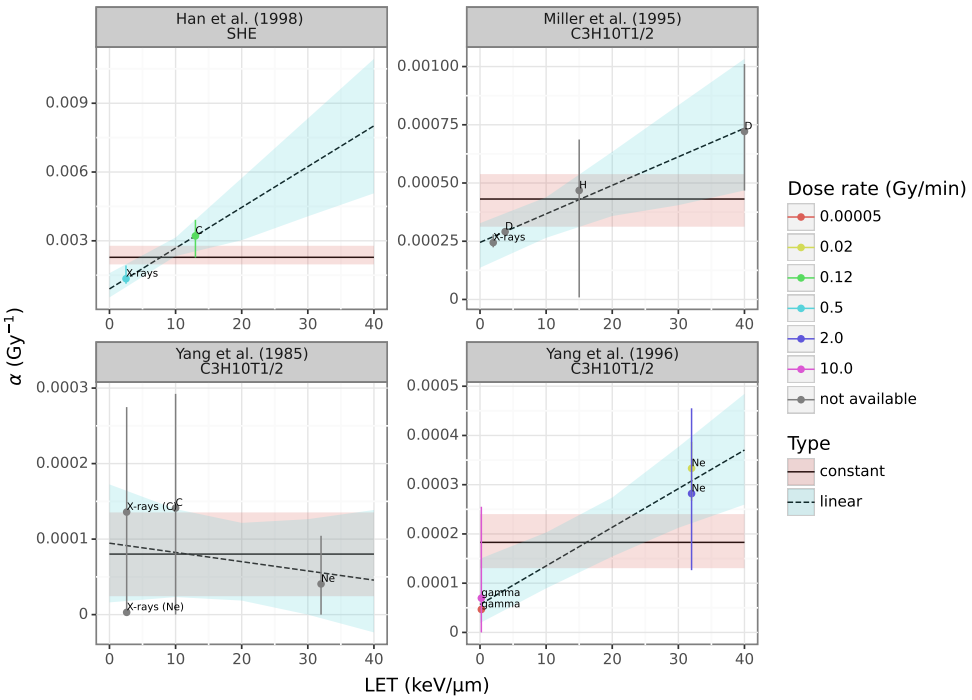

Figure 9. Linear fit of the mean of the bootstrap α as a function of LET in mutation data is shown with a dashed line. An average value of the mean of the bootstrap α is shown with a solid line. Dose rates, when available, are indicated with colours.

2.3.3 Results of the Linear Quadratic Fits and α_0 and β_0 Parameters with Dose Rate Analysis

Linear quadratic fits with dose rate of the survival data grouped by publication and particle are shown in figure 10. The figures include simple fits indicated with a solid line and the mean of fits utilising bootstrapping indicated with a dashed line. Corresponding fits of the mutation data are shown in figure 11.

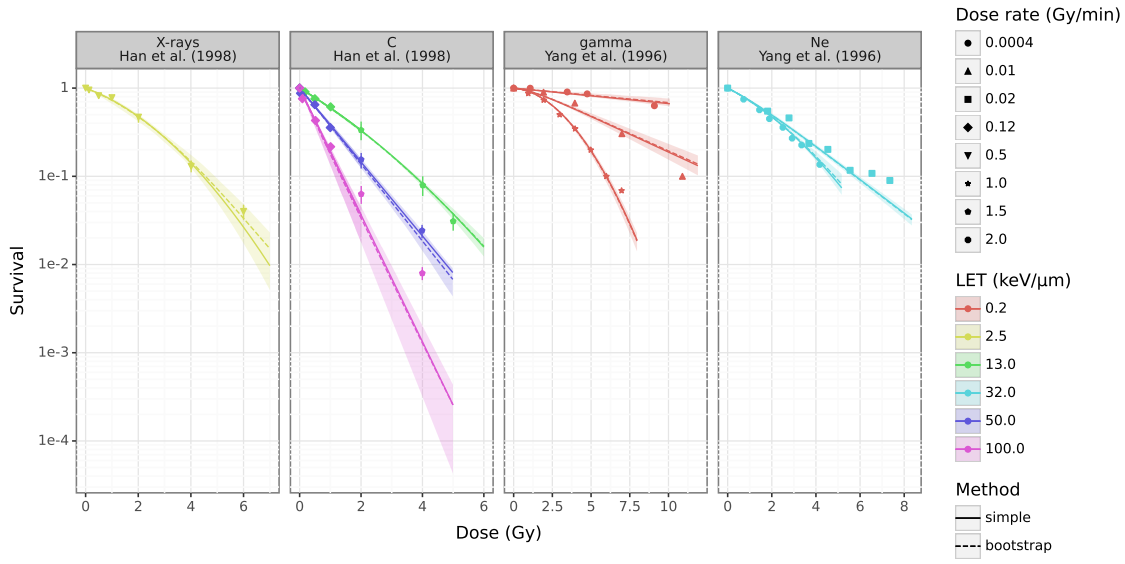

Figure 10. Fits with dose rate of the experimental *in vitro* survival data.

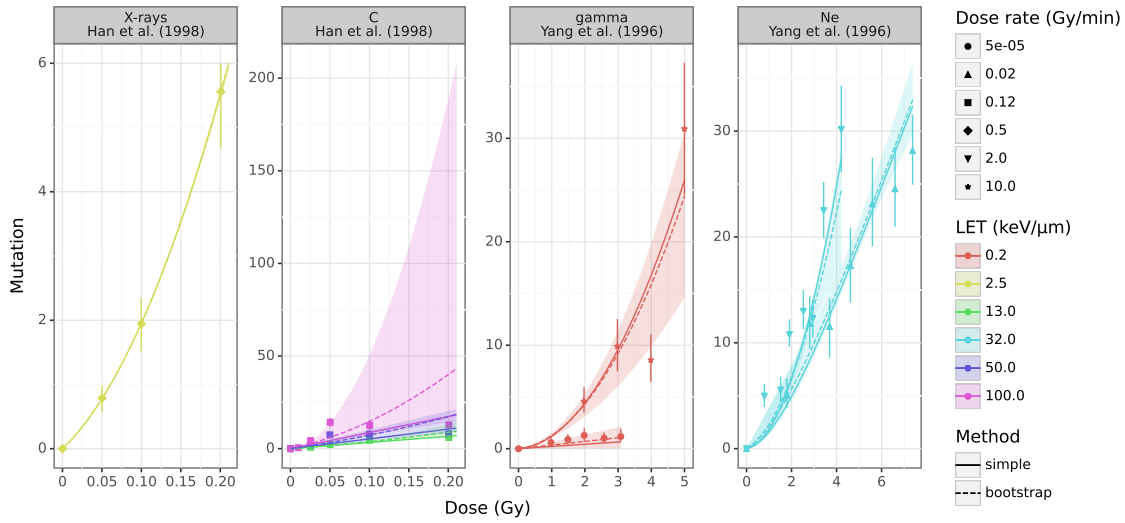

Figure 11. Fits with dose rate of the experimental *in vitro* mutation data.

Figures 12, 13 and 14 show the results of both methods, extrapolation and averaging, for finding the α_0, β_0 and τ_0 values in each survival dataset. The shaded regions represent the limits of 10 % and 90 % percentiles of the full distribution of α, β and τ obtained from bootstrapping.

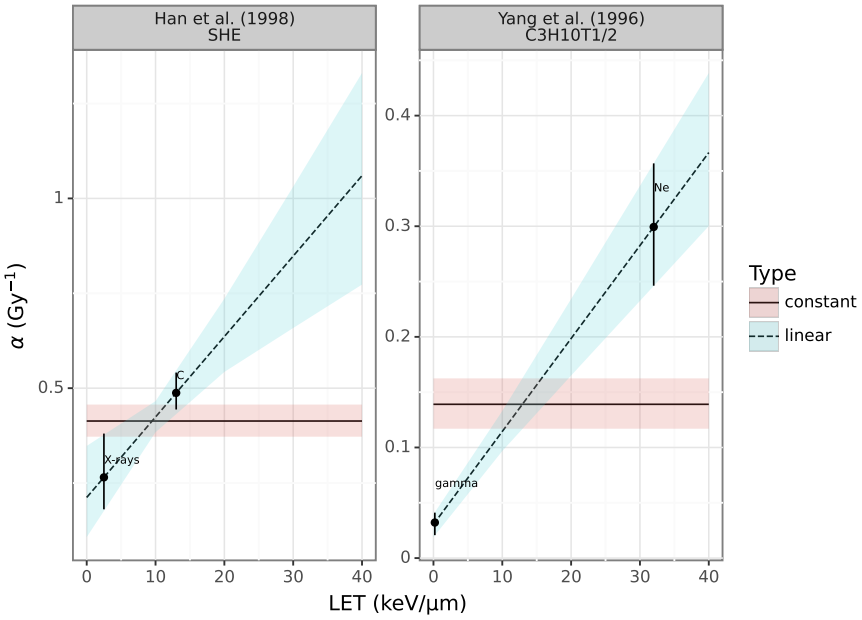

Figure 12. Linear fit of the mean of the bootstrap α as a function of LET in survival data is shown with a dashed line, covering the simple linear fit line. An average value of the mean of bootstrap α is shown with a solid line.

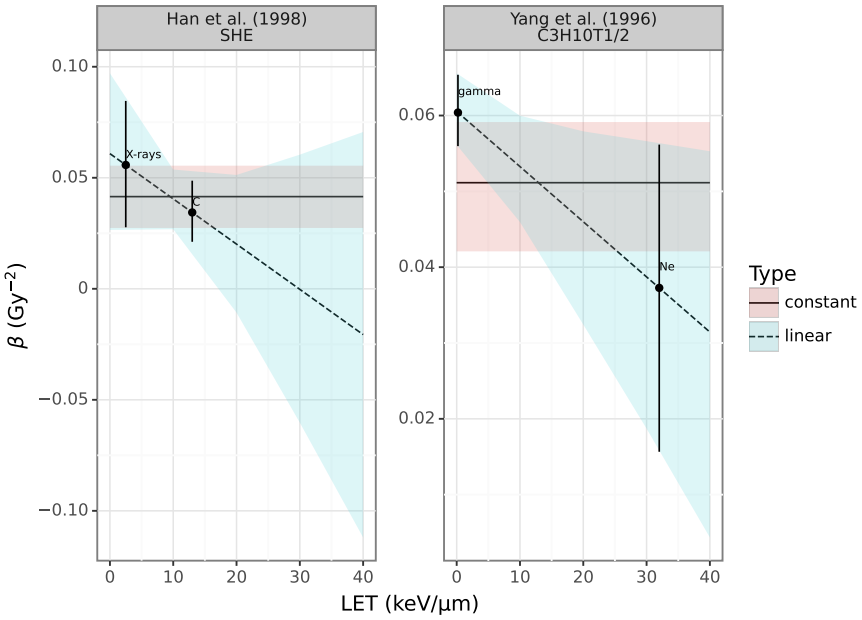

Figure 13. Linear fit of the mean of the bootstrap β as a function of LET in survival data is shown with a dashed line, covering the simple linear fit line. An average value of the mean of bootstrap β is shown with a solid line.

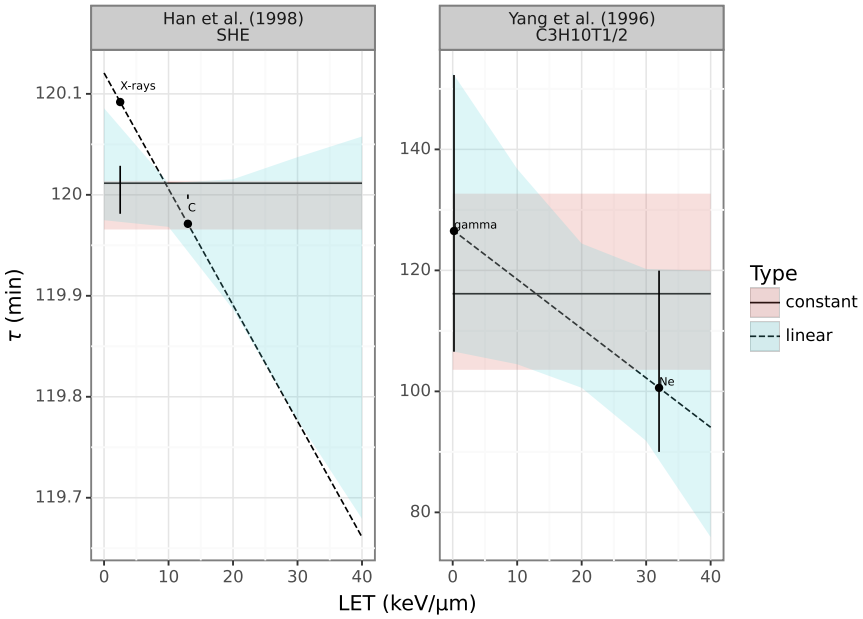

Figure 14. Linear fit of the mean of the bootstrap τ as a function of LET in survival data is shown with a dashed line, covering the simple linear fit line. An average value of the mean of bootstrap τ is shown with a solid line.

Corresponding results of the mutation data are shown in figures 43, 44 and 45 in Appendix.

2.3.4 Experimental and Theoretical Comparisons Without Taking the Dose Rate into Account

The extrapolated α and the average of β of the low LET data in each dataset were used as values for the α_0 and β_0 parameters in the MKM. A range of r_N and r_D values were then tested as parameters in the MKM in each dataset. The ones that minimised the difference between the cell survival in experimental data and the cell survival evaluation in the MKM simulation were chosen as the final MKM parameters. This approach is henceforth called the "extrapolation" approach. Minimisation was observed by subtracting the survival values predicted by the simulation from the experimental survival values, separately for each dataset and for a combination

of test parameters, and by squaring the result to avoid negative numbers. The combination of test parameters producing the smallest number as the result was the optimal choice.

Comparison of the experimental values of α parameter collected from the linear quadratic fits of the survival data and the α parameter produced by the theoretical survival simulation, for each particle with a particular LET, is shown in figure 15. Similar comparison of the values of the β parameter is shown in figure 46 in Appendix. The rapid analytical approach for survival (see equation (11)) removes the LET dependence of the β parameter, making β equal to β_0. This explains why the theoretical value of β is a constant.

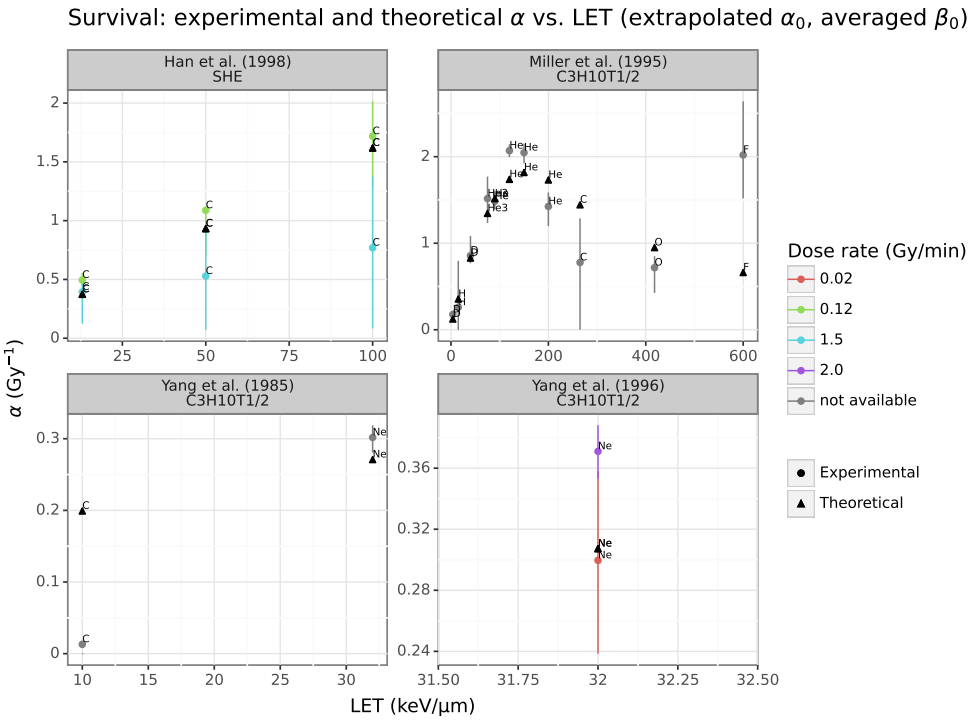

Figure 15. Experimental and theoretical values from the MKM simulation of α for survival are shown with different symbols. Parameters r_N and r_D in the MKM were optimised based on the linearly extrapolated α_0 and an average of β_0 of low LET ions. Dose rate was not included in the simulation as a parameter.

Comparison between the experimentally observed survival and survival predicted

by the MKM is shown in figure 16. The simulation used an approximation (rapid calculus), the α_0 values were obtained from linear extrapolation and the β_0 values were averaged from the low LET ions. The optimised r_N and r_D values were based on them.

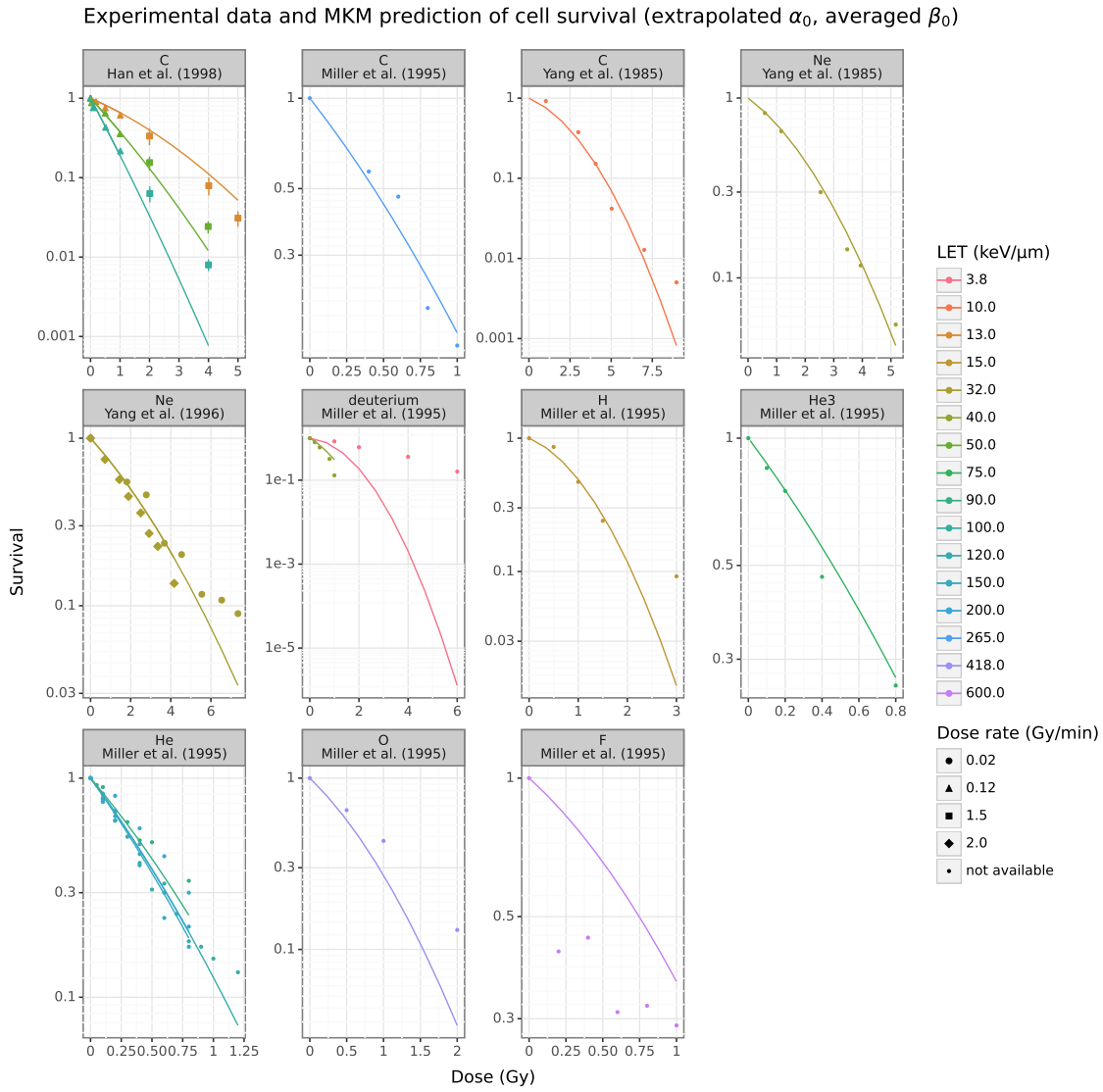

Figure 16. Experimental data are shown with data points. Survival curves as a function of dose from the MKM simulation are plotted over the experimental data points. Parameters r_N and r_D in the MKM were optimised based on the linearly extrapolated α_0 and an average of β_0 of low LET ions.

In addition, simultaneous testing of a range of α_0, β_0, r_N and r_D values was

done in each dataset. Such a combination of all four that minimised the difference between the cell survival in experimental data and in the simulation was chosen as the final MKM parameters. This alternative approach is henceforth called the "range" approach. Comparison to the experimental data was made in this case. The experimental values of α parameter collected from the linear quadratic fits of the survival data and the α parameter produced by the theoretical survival simulation, for each particle with a particular LET, are shown in figure 17. Corresponding values of the β parameter are shown in figure 47 in Appendix.

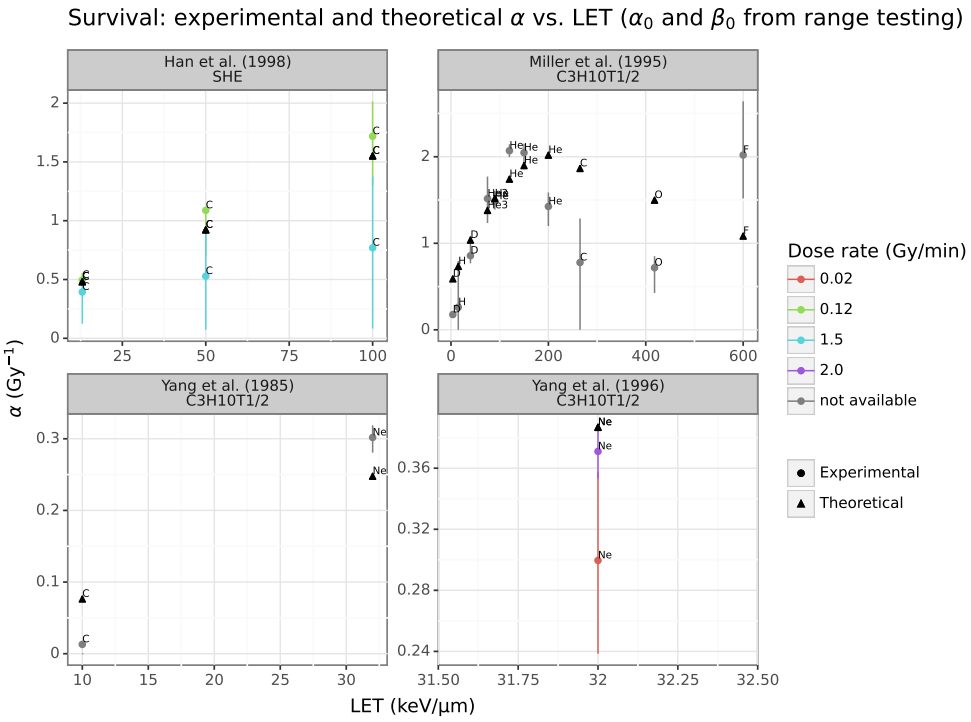

Figure 17. Experimental and theoretical values from the MKM simulation of α for survival are shown with different symbols. Parameters α_0, β_0, r_N and r_D in the MKM were optimised by testing a range of values and choosing the best fit to experimental data. Dose rate was not included in the simulation as a parameter.

Comparison between the experimentally observed survival and survival predicted by the MKM with the method of testing a range of values for all the four parameters is shown in figure 18. The simulation used an approximation (rapid calculus).

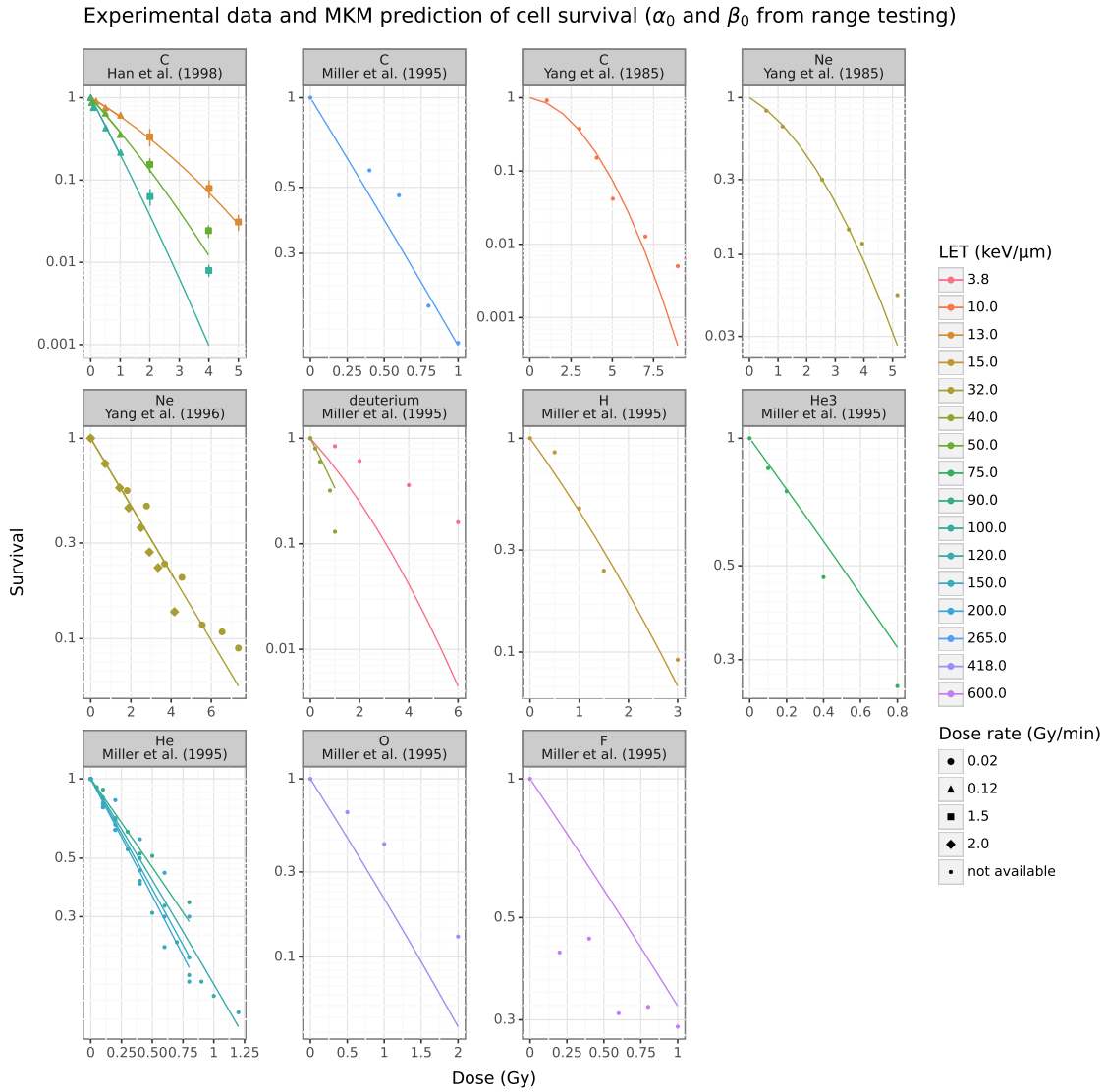

Figure 18. Experimental data are shown with data points. Survival curves as a function of dose from the MKM simulation are plotted over the experimental data points. Parameters α_0, β_0, r_N and r_D in the MKM were optimised by testing a range of values and choosing the best fit to experimental data.

In the case of mutation, the extrapolated α and the average of β of the low LET data in each dataset were used as values for the α_0' and β_0' parameters. r_N' was assumed to be the same as r_N in survival data, while a range of r_D' values were then tested as parameters in the MKM in each dataset. The one that minimised the difference between the cell mutation in experimental data and the cell mutation

evaluation in the MKM simulation was chosen as the final MKM parameter.

Comparison of the experimental values of α parameter collected from the linear quadratic fits of the mutation data and the α parameter produced by the theoretical mutation simulation, for each particle with a particular LET, is shown in figure 19. Comparison of the values of the β parameter is shown in figure 48 in Appendix.

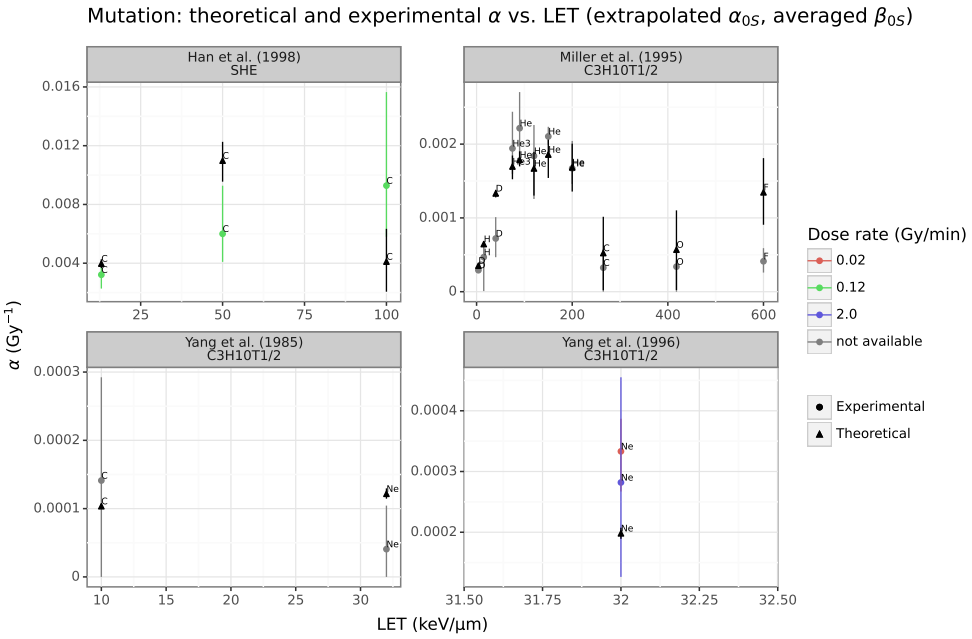

Figure 19. Experimental and theoretical values from the MKM simulation of α for mutation are shown with different symbols. Parameter r'_D in the MKM was optimised based on the linearly extrapolated α_0, linearly extrapolated α'_0, an average of β_0, and an average of β'_0 of low LET ions. Dose rate was not included in the simulation as a parameter.

Comparison between the experimentally observed mutation and mutation predicted by the MKM is shown in figure 20. The simulation used a Monte Carlo approach, and the α_0 values were obtained from linear extrapolation and the β_0 values were averaged from the low LET ions both in the case of survival and mutation.

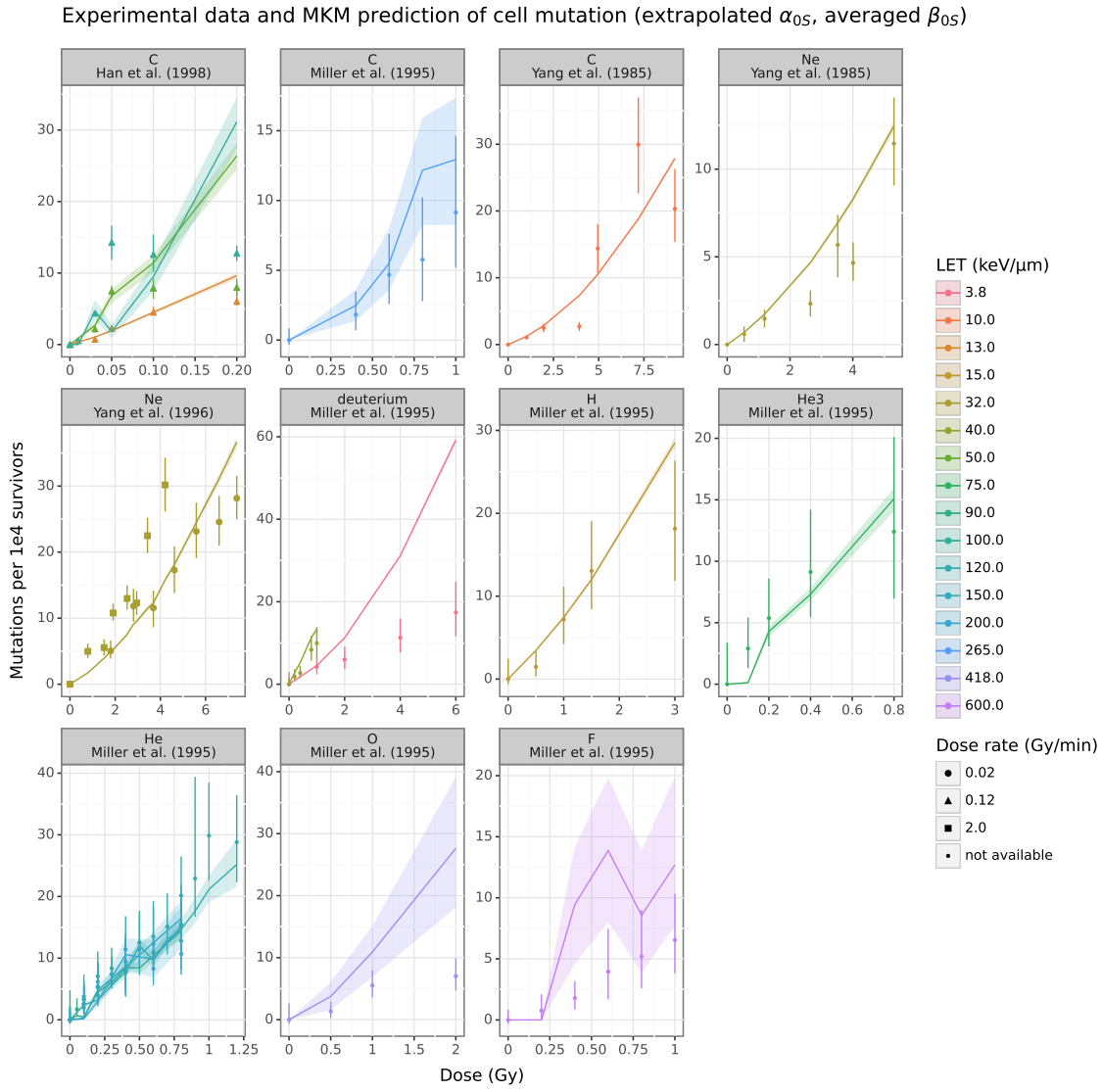

Figure 20. Experimental data are shown with data points. Mutation curves as a function of dose from the MKM simulation are plotted over the experimental data points. Parameter r'_D in the MKM was optimised based on the linearly extrapolated α_0, linearly extrapolated α'_0, an average of β_0, and an average of β'_0 of low LET ions.

Comparisons between the experimental data and the MKM prediction, where all the survival parameters were gained with the method of testing a range of values, are shown in figures 21, 49 in Appendix and 22. The α'_0 values for mutation were obtained from linear extrapolation and the β'_0 values for mutation were averaged from the low LET ions. The simulation used a Monte Carlo approach.

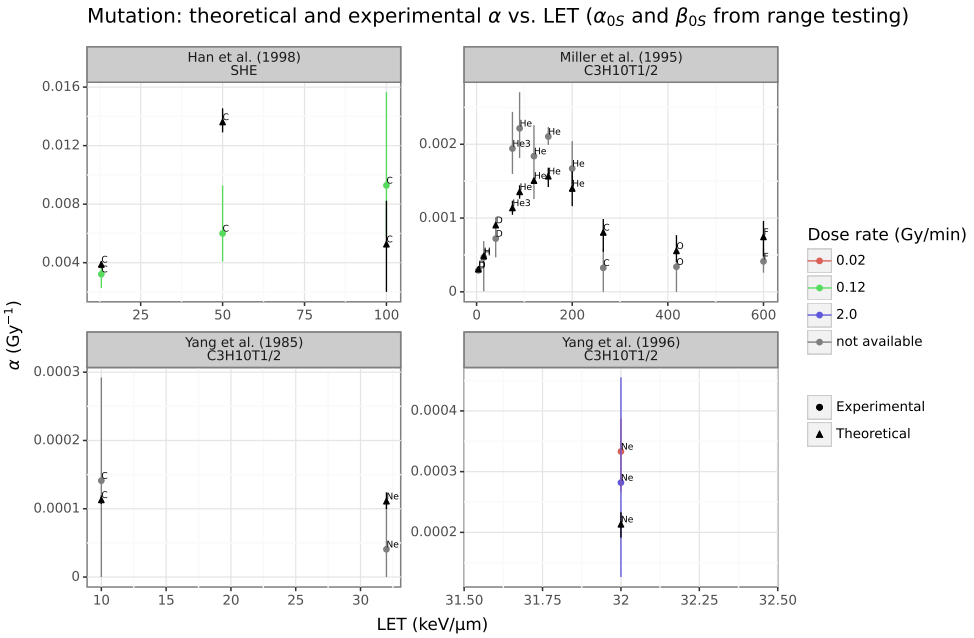

Figure 21. Experimental and theoretical values from the MKM simulation of α for mutation are shown with different symbols. Parameters α_0, β_0, r_N and r_D in the MKM were optimised by testing a range of values and choosing the best fit to experimental data, and the optimisation of the r'_D parameter was based on them. Dose rate was not included in the simulation as a parameter.

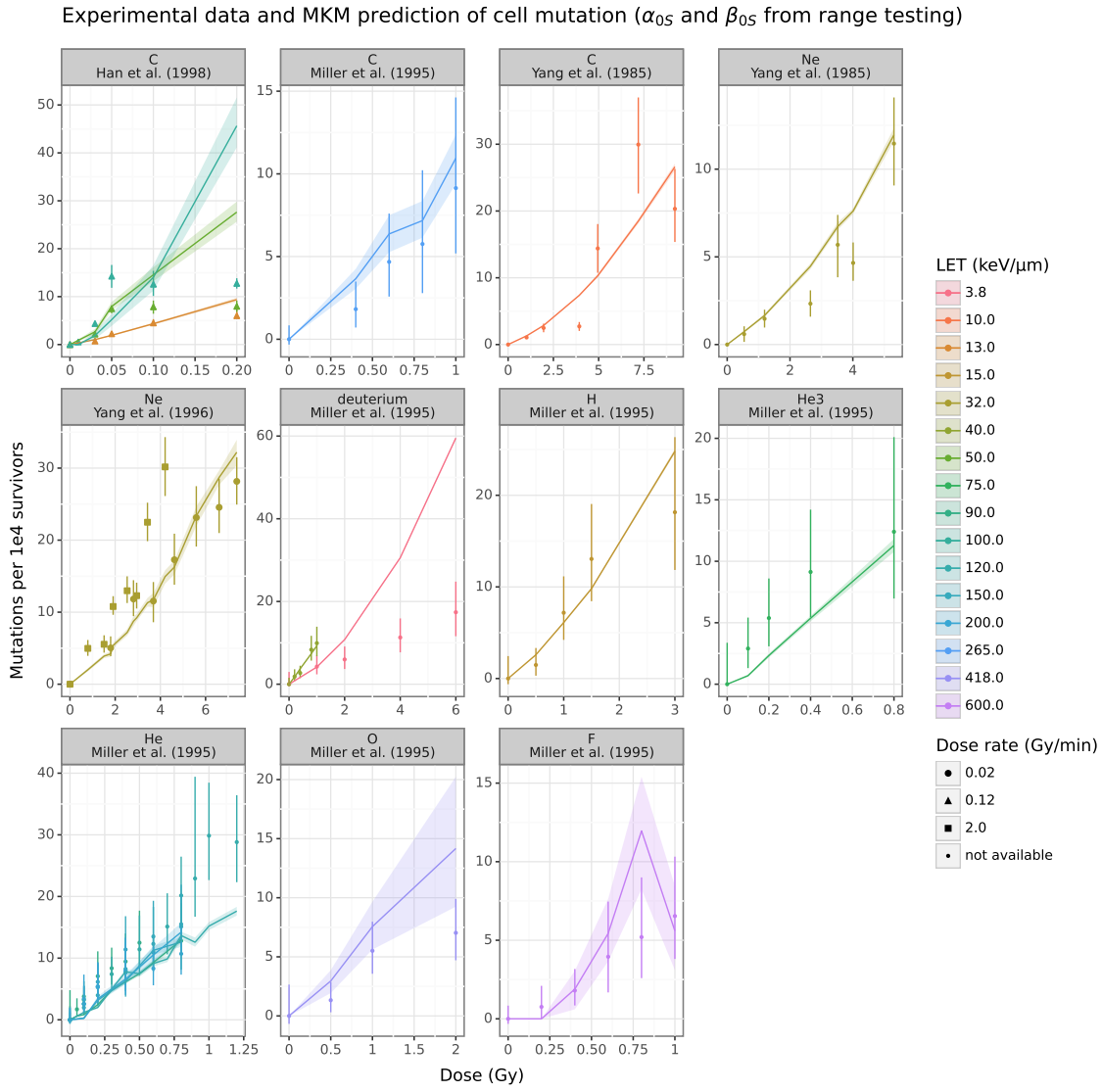

Figure 22. Experimental data are shown with data points. Mutation curves as a function of dose from the MKM simulation are plotted over the experimental data points. Parameters α_0, β_0, r_N and r_D in the MKM were optimised by testing a range of values and choosing the best fit to experimental data, and the optimisation of the r'_D parameter was based on them.

2.3.5 Experimental and Theoretical Comparisons Taking the Dose Rate into Account

In the simulation of theoretical survival and mutation curves with dose rate analysis, the α_0, β_0 and τ_0 parameters were derived from the modified linear quadratic fits

that accounted for the dose rate. As before, α_0 was taken from the extrapolation and the β_0 from the average of low LET data, both for survival and mutation. The values from the extrapolation and the average of low LET data of the new parameter τ_0 were very similar. The average was chosen. To determine r_N and r_D for survival, a range of values were tested as parameters. As before, the combination that minimised the difference between the cell survival in experimental data and in the MKM prediction was chosen as the final MKM parameters. In the case of mutation, r'_N was again assumed to be the same as r_N for survival, while a range of r'_D values were tested as parameters in the MKM simulation.

Comparison of the experimental values of α and β parameters collected from the linear quadratic fits (including the G factor) of the survival data and the α and β parameters produced by the theoretical survival simulation, for each particle with a particular LET, are shown in figures 23 and 50 in Appendix. The simulation used an approximation (rapid calculus), so there is no LET dependence for the β parameter, as in the survival analysis without dose rate dependence. An approximation was used instead of Monte Carlo because it was considerably faster to optimise.

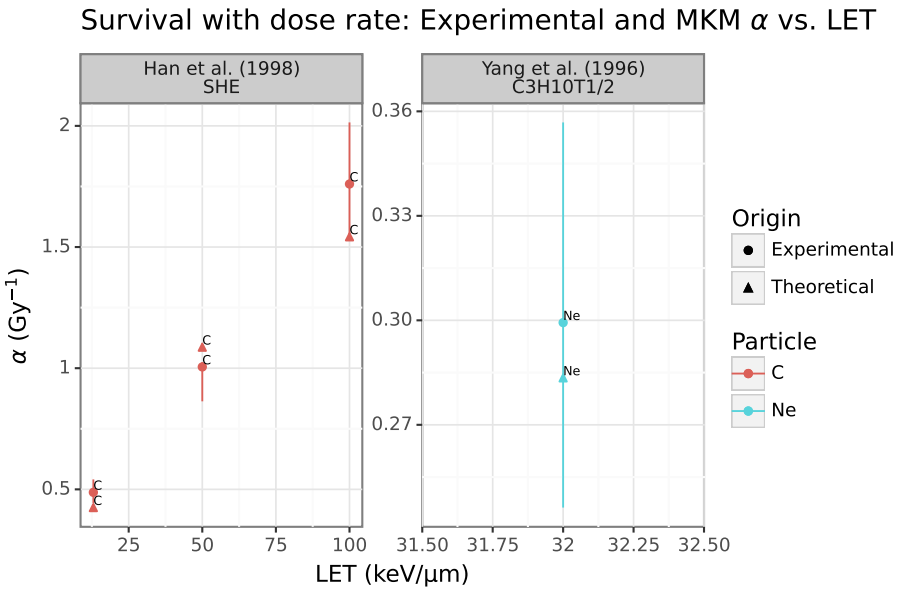

Figure 23. Experimental and theoretical values from the MKM simulation of α for survival are shown with different symbols. Parameters r_N and r_D in the MKM were optimised based on the linearly extrapolated α_0, an average of β_0, and an average of τ_0 of low LET ions.

Comparison between the experimentally observed survival and survival predicted by the MKM accounting for the dose rate is shown in figure 24. Han et al. (1998) used different dose rates for low doses and high doses. Two different MKM simulations were performed for the two subsets of data with different dose rates, resulting in different α and β values for the subsets of data. The change in dose rate is visible as a gap in the curves.

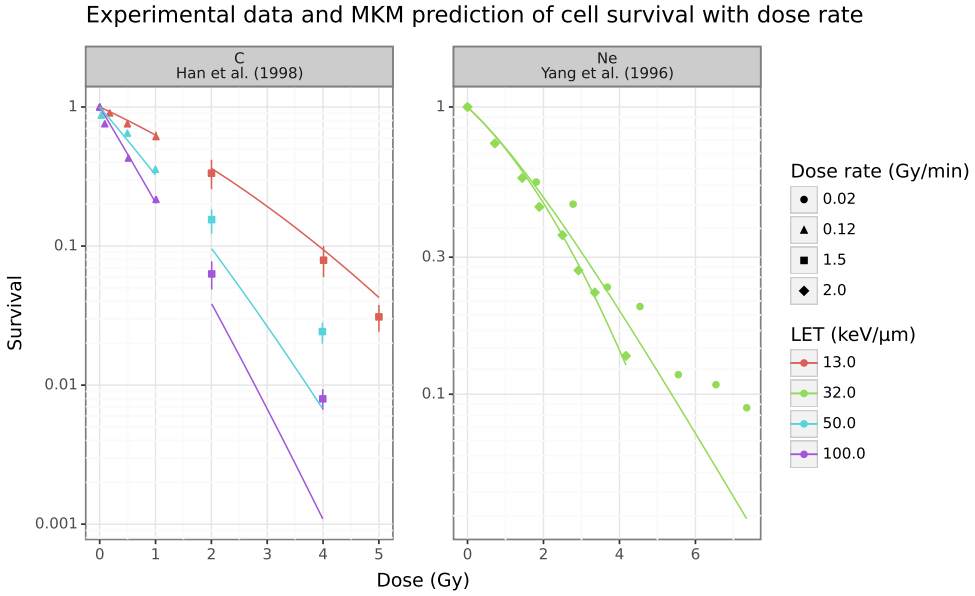

Figure 24. Experimental data are shown with data points. Survival curves as a function of dose from the MKM simulation accounting for the dose rate are plotted over the experimental data points. Parameter r_D in the MKM was optimised based on the linearly extrapolated α_0, an average of β_0, and an average of τ_0 of low LET ions.

Monte Carlo simulation of the mutation caused by low LET particles accounting for the dose rate with the modified version of the 'Survival' code proved consuming for the computer memory. The smaller the LET of the particle, the greater the number of tracks, leading to an excessive use of memory, when all the particle tracks in each domain of each cell are kept in memory. In the code not accounting for the dose rate each track has a linear contribution of dose. These doses accumulate in the cell, and the track is deleted after accumulation, freeing up the memory. Conversely, when accounting for the dose rate, the contribution to the DNA lesions from each track depends also on the previous track, and they are not deleted. The effect is evaluated based on the time difference between consecutive contributions of the tracks considering all possible pairs of tracks. In addition, higher doses require a larger number of tracks. The combination of low LET and high dose is the most memory consuming.

Further memory usage optimisation of the code is needed to compare the MKM prediction and the Yang et al. (1996) mutation dataset of two different dose rates of neon particles with LET 32 keV/μm. Han et al. (1998) dataset of carbon nuclei with LET 50 keV/μm and 100 keV/μm were completed with the current version of the code reasonably fast; the LET 13 keV/μm took the longest time to complete. While both datasets arguably include low LET values (13 and 32 keV/μm), even the smallest dose in the Yang et al. mutation data was still higher than the highest in the Han et al. mutation data, resulting in an additional use of memory in the Yang et al. dataset. The datasets have different particles, carbon and neon, so the total number of particles to simulate is different even with the same LETs.

For the Han et al. dataset, comparison of the experimental values of α and β parameters collected from the linear quadratic fits (including the G factor) of the mutation data and the α and β parameters produced by the theoretical mutation simulation, for each particle with a particular LET, are shown in figures 25 and 51 in Appendix.

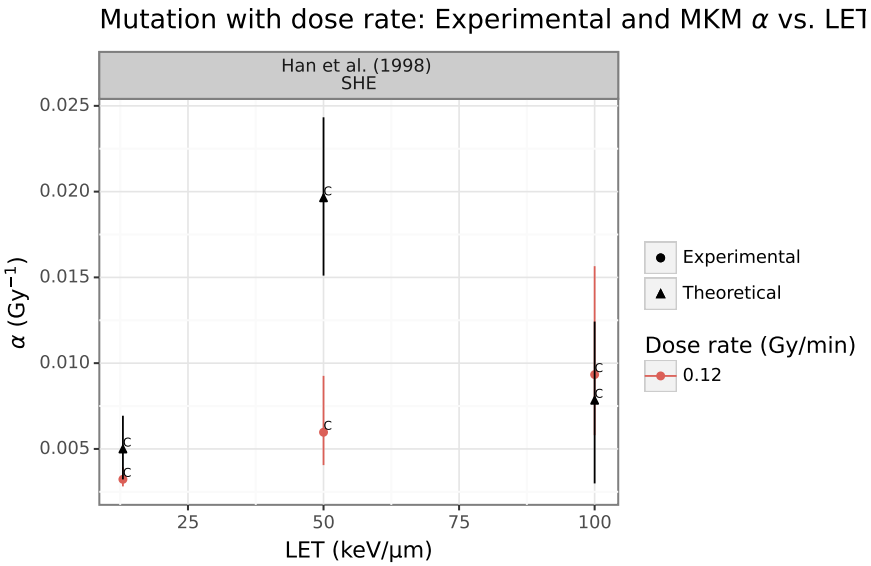

Figure 25. Experimental and theoretical values from the MKM simulation of α for mutation are shown with different symbols. Parameters r_N and r_D in the MKM were optimised based on the linearly extrapolated α_0, an average of β_0 and an average of τ_0 of low LET ions. Parameter r'_D was optimised based on the linearly extrapolated α_0, linearly extrapolated α'_0, an average of β_0, an average of β'_0, and an average of τ'_0 of low LET ions.

Figure 26 shows the comparison between experimentally observed mutation and the mutation predicted by the MKM for the Han et al. dataset. The highest dose of carbon with LET 13 keV/μm was left out of the simulation.

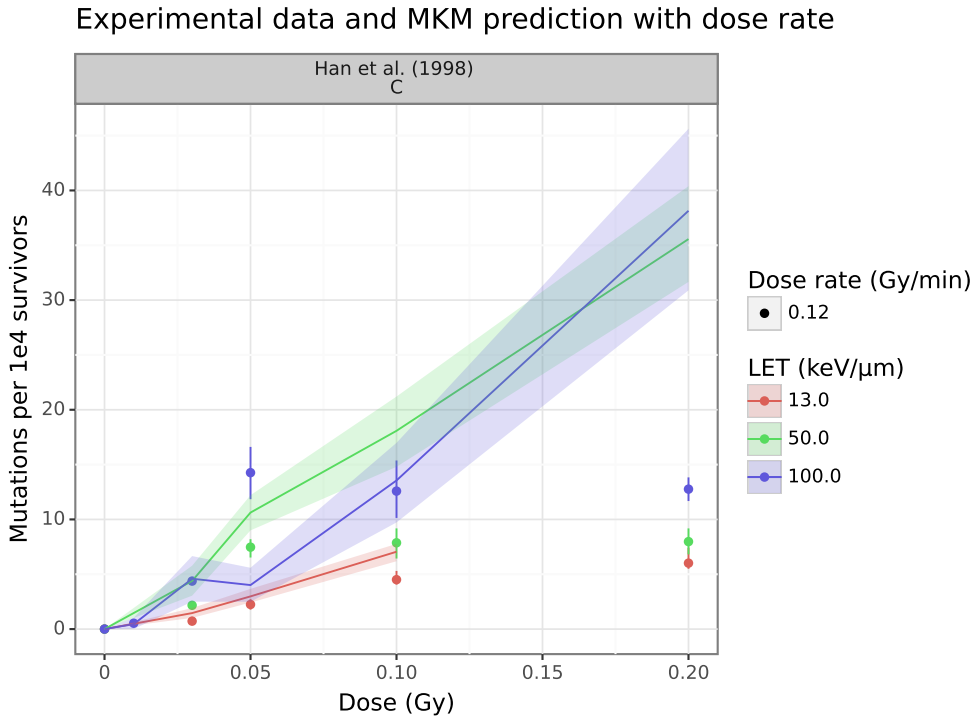

Figure 26. Experimental data are shown with data points. Mutation curves as a function of dose from the MKM simulation accounting for the dose rate are plotted over the experimental data points. Parameter r'_D was optimised based on the linearly extrapolated α_0, linearly extrapolated α'_0, an average of β_0, an average of β'_0, and an average of τ'_0 of low LET ions.

The two highest doses in the experimental Han et al. dataset diverge from linear quadratic behaviour. Therefore, another optimisation based on the comparison to the experimental data was done by excluding those data points. The resulting mutation predicted by the MKM and the comparison to the experimentally observed mutation is shown in figure 27.

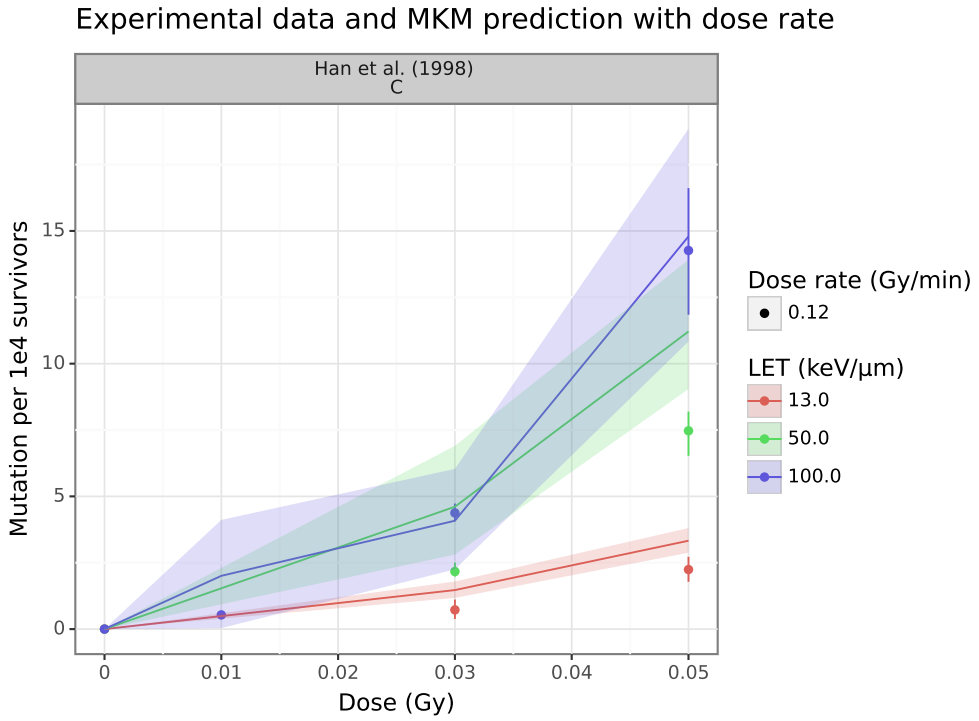

Figure 27. Experimental data are shown with data points. Mutation curves as a function of dose from the MKM simulation accounting for the dose rate are plotted over the experimental data points. Parameter r'_D in the MKM was optimised based on the linearly extrapolated α_0, linearly extrapolated α'_0, an average of β_0, an average of β'_0, and an average of τ'_0 of low LET ions.

2.4 Discussion

The low LET regions of the experimental data were better reproduced with the simulation than the high LET regions. This could indicate that the particle track model in its current form might work better for low LET than for high LET particles. In some cases, also the low dose regions were better reproduced than the high dose regions.

The mutation curves of carbon, particularly the high LET curves, in the Han et al. (1998) dataset diverge from linear quadratic behaviour. This type of divergence is unique to this experiment. In other similar experiments a universal linear quadratic behaviour is observed (McMahon, 2018). Therefore, the issues of reproducing high

LET region could also reflect some issues with the experimental data.

In the MKM simulations of survival probability, testing a range of values of all four parameters – α, β, r_N and r_D – produced results closer to the experimental datasets, when comparing the results of the whole dataset, not of each particle separately. In both approaches simulations of low LET carbon, neon, hydrogen, helium-3 and helium-4 resembled the experimental data especially in the lower doses. On the other hand, simulations of high LET carbon, deuterium, oxygen and fluorine differed from the observations. Apart from deuterium, these were all high LET particles. Assuming that the simulations are handling the isotopes correctly, the issue with deuterium could be partly associated with difficulties in the high doses region, either stemming from the experimental data or the particle track model.

Similarly, regardless of the approach, the MKM simulations of mutation probability seemed to overestimate mutation probability with high LET carbon, deuterium, oxygen and fluorine, and underestimate with helium-3 and helium-4. Mutation probability with hydrogen and lower dose rate neon resembled the experimental data quite well. The same applies to low LET carbon but only in the low dose region.

The MKM simulations of survival probability with dose rate as a parameter, based on two datasets, showed a similar trend of better resemblance to the experimental data in the low LET region. In the two lowest LETs, 13 keV/μm carbon and 32 keV/μm neon, the resemblance was good in all the doses. The higher LETs, 50 keV/μm and 100 keV/μm carbon, produced good resemblance in the lower doses but began to underestimate survival probability in the higher doses. The same trend was observed when comparing to the simulations of these same particles without the dose rate as a parameter. The MKM simulation of mutation probability with dose rate as a parameter, based on one dataset, likewise produced a better resemblance to the experimental data in the low LET and low dose region. However, the

prediction resemblance improved for the high LET particles, when the highest dose points diverging from the linear quadratic behaviour in the experimental dataset were removed.

Currently 'Survival' code accepts only singular values of α and β parameters as input. This assumes every cell has the same sensitivity to radiation. However, there might be differences between the cells. For example, spontaneous mutations occurring in the cells can modulate the cells' sensitivity to radiation. Therefore, using a distribution of α and β values as parameters might produce more accurate results. As noted, the particle track model could perhaps also be improved.

To optimise the use of memory in the analyses accounting for the dose rate, the dose contribution of the tracks before any given current track being analysed could be accumulated and afterwards deleted. This would speed up the analyses even for the high LET particles, even though the actual challenge is in the low LET particles with a vast number of particle tracks.

3 Characterisation of Space Radiation Environment on Mars

3.1 Theoretical Background

3.1.1 Radiation Environment on Mars

Mars has a harsher radiation environment compared to Earth. First, Mars does not have a global magnetic field that would shield the planet from energetic charged particles (Acuña et al., 1998). Second, the atmosphere is thinner. Maximum atmospheric density on the surface of Mars is approximately 20 g/m^3, like Earth's atmospheric density at 35 km. The lower atmosphere on Mars is mostly composed of CO_2 ($95 - 96$ %), nitrogen, argon, oxygen and CO. The upper atmosphere at $80 - 1000$ km altitude has three layers: ionosphere, thermosphere and exosphere. The ionosphere from 80 km to $500 - 600$ km has its peak ion concentration of 10^5 cm^{-3} just below 130 km, consisting 90 % of O_2^+ and 10 % of CO_2^+ ions. (Mahaffy et al., 2013; Mangold et al., 2016)

Mars is hit by energetic particle radiation originating both from SPEs and GCRs. Column depths of the Martian atmosphere are approximately 20 g/cm^2 and typically ions with energies below 150 MeV/nuc lose their energy before reaching the surface. However, the particles that are energetic enough not only penetrate the atmosphere but can also penetrate several metres into the regolith producing secondary particles, further adding to the radiation exposure. (Hassler et al., 2014)

3.2 Methodology

3.2.1 OLTARIS Simulations

OLTARIS (On-Line Tool for the Assessment of Radiation in Space) was used to obtain the space radiation conditions and its effects on humans on a habitat on

Mars. Based on the input data, OLTARIS assesses the SPE and GCR environment on Mars surface at a given site. OLTARIS uses HZETRN (High Charge [Z] and Energy Transport) and NUCFRG3 (Nuclear Fragmentation 3) computer codes that have been developed by the NASA Langley Research Center. (Singleterry et al., 2010)

The site in this study was chosen to be the landing site of the rover Persistence in NASA's Mars 2020 mission, Jezero crater, at latitude 18.44°N and longitude 77.45°E. Elevation on Mars is measured against the equipotential surface, Mars areoid, which is analogous to Earth geoid, in essence sea level. Computations utilising both the geometry and the gravity potential value of the areoid represent the equipotential surface as the surface of a liquid Mars in hydrostatic equilibrium (Ardalan et al., 2010). Surface elevations vary from minus 10000 metres to 30000 metres. The floor of the Jezero crater is at minus 2600 metres.

The environment conditions were determined for calculations of the radiation spectrum on the Mars surface with OLTARIS. Surface parameters were based on the Mars Climate Database (MCD). Calculations were done with the NASA design standard SPE for missions beyond Earth orbit and the Badhwar-O'Neill 2010 model of the 2010 solar minimum galactic cosmic radiation. The design SPE is the sum of the proton spectra for the events that occurred between October 19 and 24, 1989, as represented by the Band function parametrization of Tylka et al. (2010) and proposed by Townsend et al. (2018). The October 1989 SPEs are among the largest events to have occurred during the solar cycle 22 (Lario et al., 2001). To assess the maximum risk worse radiation conditions were chosen over favourable ones. Therefore, in the assessment of GCR environment, solar minimum was chosen over solar maximum, as during a maximum the outward expanding solar wind results in a lower GCR density in the heliosphere.

The stay on the planet surface was initially defined for 30 days. The doses

received from the example SPE were observed for different times, ranging from 1 to 400 hours. For the habitat, a three-dimensional material thickness distribution of a sphere made of 5 g/cm^2 polyethylene was chosen. The choice was based on assessment of different shielding configurations and their effectiveness at different surface elevations in a study by Ortiz et al. (2015), where 5 g/cm^2 polyethylene was considered suited to serve as a primary radiation storm shelter on Mars below 11 km elevation. In the computational analyses of the study the permissible exposure limits defined by NASA were not exceeded. Polyethylene provides better shielding from radiation than the mere atmosphere.

For SPEs, OLTARIS determined the fluence, referring to the number of incident particles crossing a plane of unit area, their type, and energy at a target point 1 m above the planet surface at a given location. An example of particle fluence vs. energy is shown in figure 52 in Appendix. For GCRs, OLTARIS determined the flux, referring to the rate of flow of particles through a unit area, their type, and energy at the same target point. An example of particle flux vs. energy is shown in figure 53 in Appendix.

3.2.2 Cell Survival and Mutation on a Mars Mission

'Survival' code can be used for evaluations of mixed radiation fields. Multiple ions with multiple energies can be described in an external file created by the user, by including information about particle type, charge, atomic number, either energy or LET (only one of them is needed) and weight, which refers for example to the flux or the fluence of the particles. It should be noted that the results presented here utilising the code in the evaluation of a mixed radiation field are preliminary in nature, and that this feature of the code is undergoing improvements.

In this study, part of the data – particle type, energy and flux or fluence – to characterise the radiation spectrum on a site on Mars was obtained from OLTARIS.

The charges of the ions and their atomic numbers are known, so they were added to the spectrum description. The MKM simulations of cell survival and mutation were then carried out for the SPE spectrum using the optimised parameters discovered from the linear quadratic fits and the comparisons to experimental data, as shown in the previous analysis. First, simulations not accounting for the dose rate were carried out with the original formulation of the 'Survival' code. Then, simulations accounting for the dose rate were carried out with the modified version of the code.

Finally, to compare the radiation exposure with the permissible exposure limit for non-cancer effects expressed as an equivalent dose in the NASA Technical Standard document on crew health (NASA, 2023), the RBE values were estimated. The document states the recommended RBE for non-cancer effects used in the equivalent dose calculations is 1.5 for protons with energies over 2 MeV and 2.5 for heavy ions. However, the MKM simulations have a different endpoint, so the comparison to the NASA limit is qualitative, not quantitative. The MKM simulations predict the probabilities of cell survival and observable mutations, rather than non-cancer effects, and use parametrizations based on the experimental datasets. The RBE values were determined separately for each dataset as the ratios between the α values of the MKM simulations indicating radio sensitivity and the α_X values of the experimental X-rays (or gamma rays in the case of Yang et. al, 1996). These α values for survival were derived from the linear quadratic fits of the survival probability as a function of dose. Similarly, the α' values for mutation were derived from the linear quadratic fits of the probability of observable mutation as a function of dose. To obtain the equivalent doses, the RBE values were then multiplied with the physical doses that the astronauts would be exposed to during an SPE.

SPEs in October 1989 lasted for approximately five days from October 19 to 24. However, looking at the event profile in figure 28, the effective duration of the events is closer to 50 hours. The total dose resulting from the event was calculated

in OLTARIS to be 29.81 mGy. Because the present implementation of the code includes data of the stopping power vs. energy from proton to neon, particles heavier than neon were excluded from the simulation. The total dose included in the simulation estimated from the LETs and the fluence of the particles was 28.51 mGy. This means over 95 % of the dose is already accounted for in the ions from proton to neon. Dose received in one hour was approximated as the total dose divided by 50 hours, although the flux is not constant during the whole event.

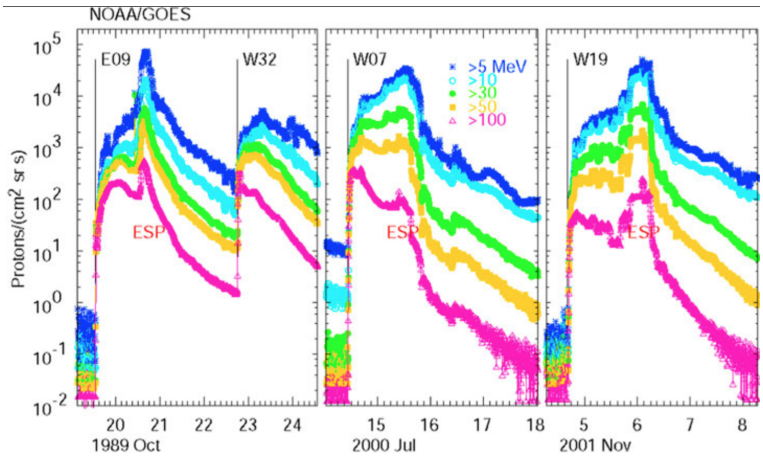

Figure 28. The intensity-time profiles of protons for different energy channels taken from Reames (2023). The first figure shows the series of SPEs in October 1989. Only the energy channel above 100 MeV includes protons with energies high enough to reach the surface of Mars. ESP refers to "energetic storm particles".

In the case of GCRs, the dose per day was calculated in OLTARIS to be 6.806 mGy in 30 days or 0.2269 mGy per day. When ions heavier than neon were excluded, the total dose estimated from the LETs and the flux of the particles was 5.1906 mGy in 30 days or 0.1730 mGy per day. Thus approximately 76 % of the dose is accounted for in the ions from proton to neon. Therefore, subsequent analysis focused on the radiation spectrum of the SPE with over 95 % dose inclusion in the MKM simulation.

3.3 Results

The probability of cell survival predicted by the MKM simulation as a function of dose is shown in figure 29. Figure 30 shows the probability of observable mutation as a function of dose. In both cases, the first dose point corresponds to a dose received in one hour, 0.570 mGy. The other points correspond to 50, 100, 150, 200, 250, 300, 350 and 400 hours, where 50 hours reflects the effective duration of the SPE. The simulation was repeated eight times using the parameters from all the four experimental datasets and from both approaches of optimising α_0 and β_0 values, extrapolation and range, as previously described. Dose rate was not included as a parameter in the simulations.

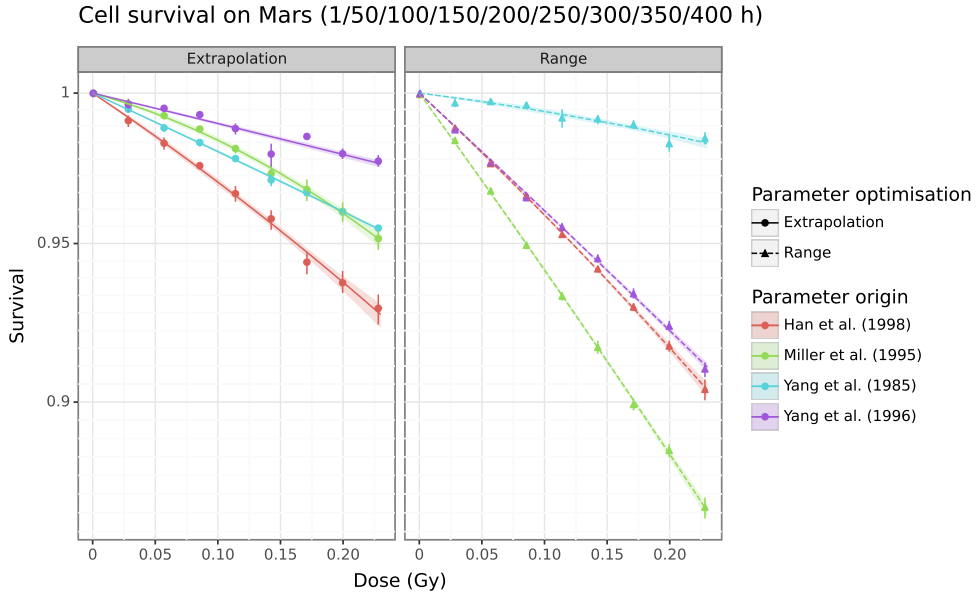

Figure 29. The probability of cell survival predicted by the MKM simulation as a function of dose. The dose points correspond to a dose received in 1, 50, 100, 150, 200, 250, 300, 350 and 400 hours.

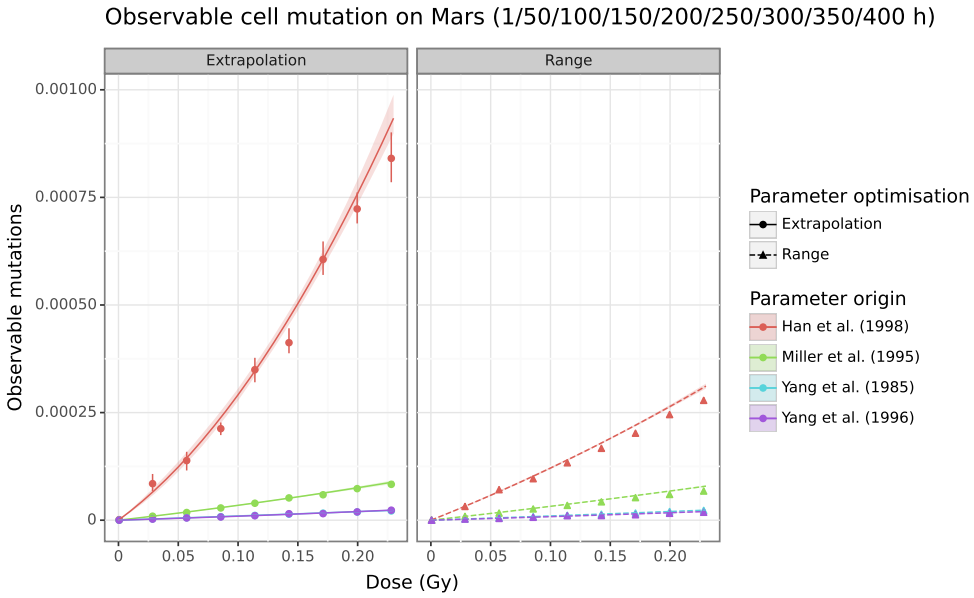

Figure 30. The probability of observable mutation per cell predicted by the MKM simulation as a function of dose. The dose points correspond to a dose received in 1, 50, 100, 150, 200, 250, 300, 350 and 400 hours.

The calculated RBE values are shown in table II. The values obtained from the experimental X-ray measurements were for the most part within the range of other *in vitro* data research for neoplastic transformations. The Yang et al. (1996) dataset used gamma ray measurements instead of X-rays, and the calculated RBE values were much higher. This is at least partially to be expected due to a lower α value.

The probability of cell survival predicted by the MKM simulation as a function of equivalent dose (obtained by multiplying the doses with the RBE values) is shown in figure 31. Figure 32 shows the probability of observable mutation as a function of equivalent dose. In both cases, the first dose point corresponds to a dose received in one hour, 0.570 mGy. The other points correspond to 50, 100, 150, 200, 250, 300, 350 and 400 hours, where 50 hours reflects the effective duration of the event. The simulation was repeated eight times using the parameters from all the four experimental datasets and from both optimisation approaches. Dose rate was not included as a parameter in the simulations. NASA's 30-day dose limit for

career/non-cancer effects is the lowest for blood-forming organs and the circulatory system, 250 mGy-Eq. This equivalent dose is marked in the figures.

Table II. Calculated RBE values of each dataset. RBE_S is calculated from survival data and RBE_M from mutation data.

Dataset	RBE_S		RBE_M	
	Extrapolation	Range	Extrapolation	Range
Han et al. (1998)	1.064	1.484	1.550	0.803
Miller et al. (1995)	0.918	4.654	1.395	1.273
Yang et al. (1985)	0.808	0.220	1.421	1.430
Yang et al. (1996)	3.198	12.352	2.812	2.300

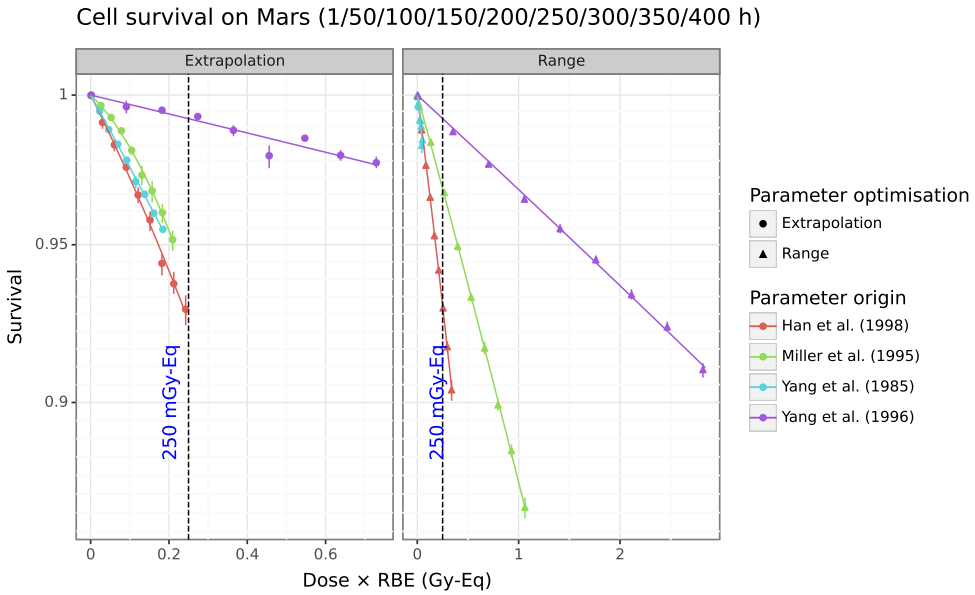

Figure 31. The probability of cell survival predicted by the MKM simulation as a function of equivalent dose. The dose points correspond to a dose received in 1, 50, 100, 150, 200, 250, 300, 350 and 400 hours. NASA's 30-day dose limit of 250 mGy-Eq for career/non-cancer effects for the blood-forming organs and the circulatory system is marked with a vertical line.

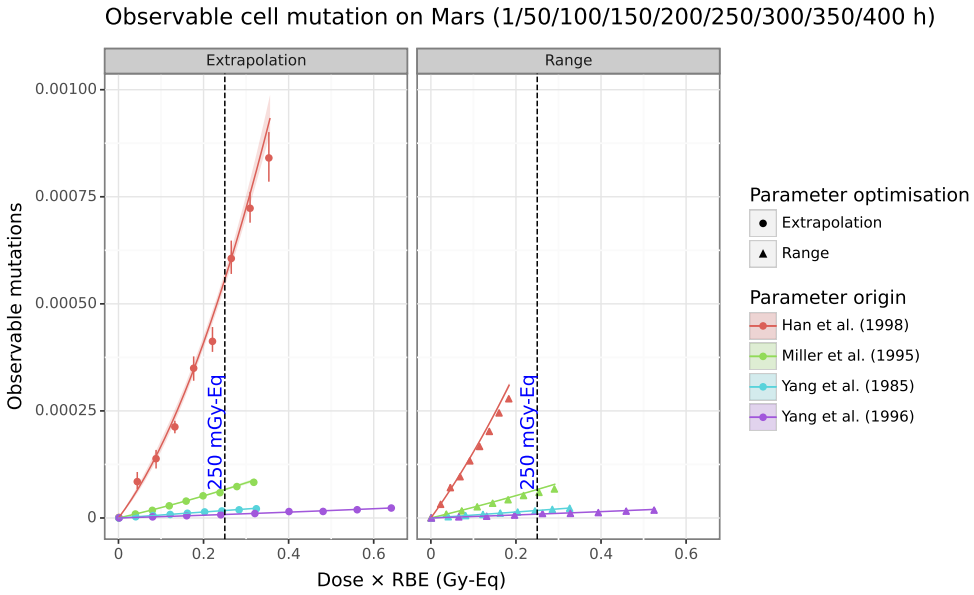

Figure 32. The probability of observable mutation per cell predicted by the MKM simulation as a function of equivalent dose. The dose points correspond to a dose received in 1, 50, 100, 150, 200, 250, 300, 350 and 400 hours. NASA's 30-day dose limit of 250 mGy-Eq for career/non-cancer effects for the blood-forming organs and the circulatory system is marked with a vertical line.

MKM simulations for survival and mutation accounting for the dose rate were also carried out using the modified version of the 'Survival' code. The parameters were taken from the dose rate fit and optimisation with the Han et al. (1998) dataset, as outlined in chapters 2.2.5 and 2.3.5. Due to the excessive use of memory in the dose rate simulations, the simulations were carried out for smaller doses, namely doses received in 1–5 hours instead of 1–400 hours. To investigate the effect of the dose rate to the results, another MKM simulation with the original version of the 'Survival' code but otherwise with the same parameters – with the exclusion of dose rate as a parameter – was carried out. Figure 33 shows the results of both approaches for the probability of cell survival predicted by the MKM simulation as a function of dose. Similarly, figure 34 shows both results for the probability of observable mutation as a function of dose.

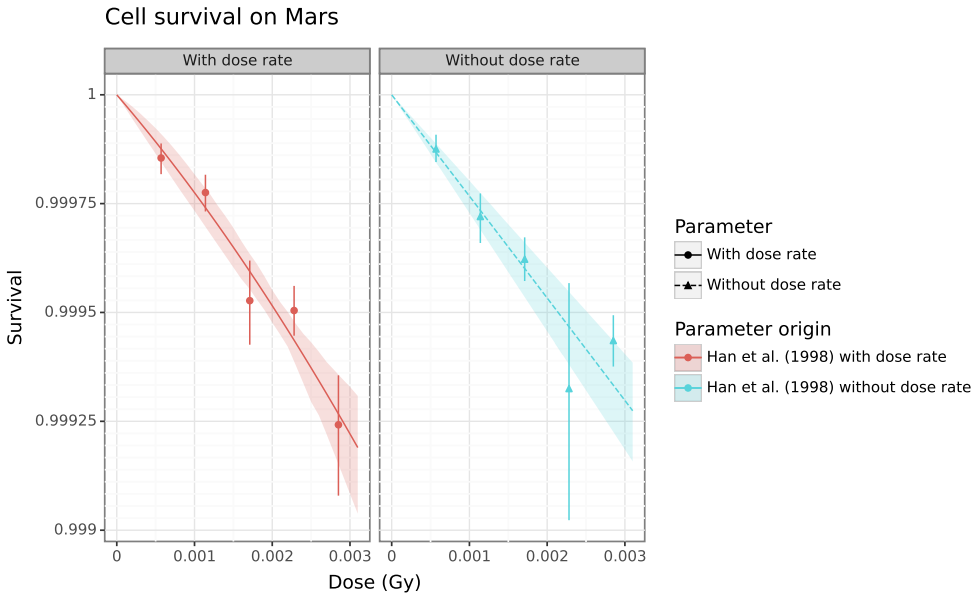

Figure 33. The probability of cell survival predicted by the MKM simulation as a function of dose. The dose points correspond to a dose received in 1, 2, 3, 4 and 5 hours.

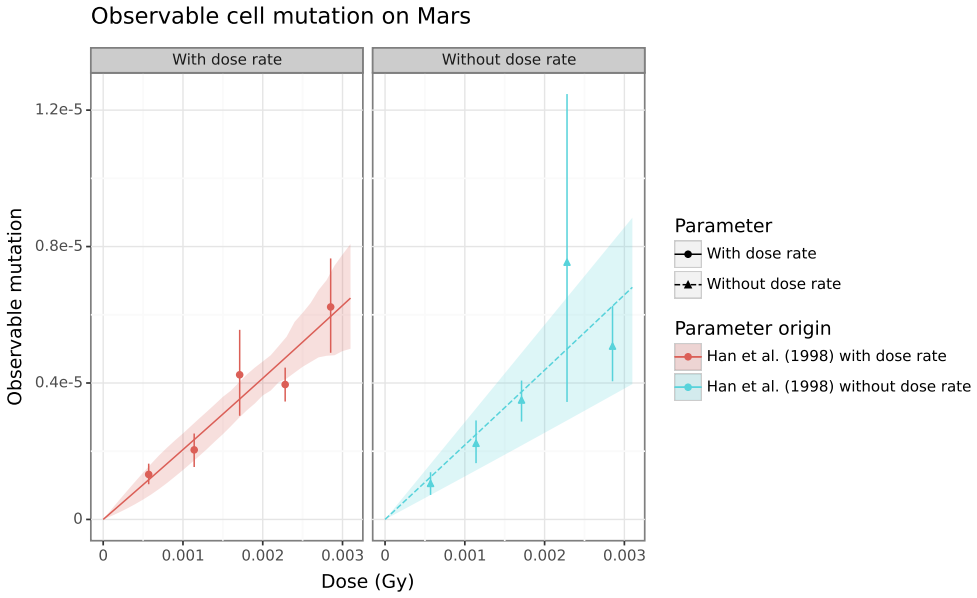

Figure 34. The probability of observable mutation per cell predicted by the MKM simulation as a function of dose. The dose points correspond to a dose received in 1, 2, 3, 4 and 5 hours.

3.4 Discussion

The dataset the parametrization was based on influenced the predicted cell survival, as did the approach – extrapolation or range – to obtain the parametrization. In the prediction of observable cell mutation different parametrizations from different datasets but within the same cell line C3H10T1/2 produced similar results regardless of the approach. Another cell line SHE produced different results compared to C3H10T1/2, as well as within the SHE cell line with different approaches. This means the choice of parametrization is an important step in the predictions of the MKM simulations.

In the probability predictions vs. dose × RBE, the simulation based on parameters from the Yang et al. (1996) dataset differed from the others likely due to the use of gamma rays instead of X-rays as the reference radiation for the calculated RBE values. In the case of cell survival, the simulations with parameters based on the other datasets, depending on the parameter optimisation approach (extrapolation or range), predicted exceeding the NASA's 30-day dose limit (250 mGy-Eq for career/non-cancer effects for the blood-forming organs and the circulatory system) earliest at 100 hours or even only after 400 hours of exposure to the design SPE. In the case of observable mutation vs. dose × RBE, the simulations predicted crossing the limit between 250–350 hours or only after 400 hours of exposure. In this qualitative comparison to the equivalent dose limit, and with the assumption that the SPE effective duration was 50 hours, it is safe to say that the exposure levels would not be expected to continue as high throughout those times.

Including the dose rate as a parameter made only a small difference in the MKM predictions of survival and observable mutation in the low doses.

4 Conclusions

This study presented methods to evaluate carcinogenic mutations in cells caused by ionising radiation using the MKM, starting from defining the parameters of the model based on a subset of the available experimental data, comparing the results of the model with the full set of available experimental data, and ending with extrapolations to evaluations for a set of space mission scenarios. The methods presented in this thesis could assist in the evaluation of carcinogenic mutations caused by ionising radiation, including the effects of radiation on a space mission.

While the probability of observable mutation at a cell level does not directly equate to the probability of cancer, it is the first step in modelling cancer risk. Currently the model simulations have a higher resemblance to experimental data in the low LET and low dose regions than in the high LET and high dose regions. Improvements for the model simulations suggested in the discussion of chapter 2 as well as improvements in the choice of parameters could lead to even better agreement between the model prediction and experimental data.

Many factors add to the complexity of mutation prediction, dose rate being one of them. In this work, when dose rate was accounted for in the analysis, there was only a small difference to the analysis without dose rate. This is expected for the low doses, whereas a higher dose rate effect is expected for higher doses. Dose rate should therefore be further explored in future research of space radiation effects.

Acknowledgements

The author is thankful for the supervision of Dr. Andrea Attili and for the additional supervision of Prof. Maurizio Marrale and Dr. Philipp Oleynik. The author acknowledges the use of computational resources in the framework of the Finnish Grid Computation Infrastructure.

References

Acuña, M. H., Connerney, J. E. P., Wasilewski, P., Lin, R. P., Anderson, K. A., Carlson, C. W., McFadden, J., Curtis, D. W., Mitchell, D., Reme, H., Mazelle, C., Sauvaud, J. A., d'Uston, C., Cros, A., Medale, J. L., Bauer, S. J., Cloutier, P., Mayhew, M., Winterhalter, D., & Ness, N. F. (1998). Magnetic Field and Plasma Observations at Mars: Initial Results of the Mars Global Surveyor Mission. *Science*, *279*(5357), 1676–1680.

Ardalan, A. A., Karimi, R., & Grafarend, E. W. (2010). A New Reference Equipotential Surface, and Reference Ellipsoid for the Planet Mars. *Earth, Moon, and Planets*, *106*(1), 1–13.

Attili, A., Scifoni, E., & Tommasino, F. (2022). Modelling the HPRT-gene mutation induction of particle beams: Systematic in vitro data collection, analysis and microdosimetric kinetic model implementation. *Physics in medicine & biology*, *67*(19), 195001.

Borek, C., Hall, E. J., & Rossl, H. H. (1978). Malignant Transformation in Cultured Hamster Embryo Cells Produced by X-rays, 430-keV Monoenergetic Neutrons, and Heavy Ions. *Cancer Research*, *38*, 2997–3005.

Brenner, D. J., Hlatky, L. R., Hahnfeldt, P. J., Huang, Y., & Sachs, R. K. (1998). The Linear-Quadratic Model and Most Other Common Radiobiological Models Result in Similar Predictions of Time-Dose Relationships. *Radiation Research*, *150*, 83–91.

Chancellor, J., Nowadly, C., Williams, J., Aunon-Chancellor, S., Chesal, M., Looper, J., & Newhauser, W. (2021). Everything you wanted to know about space radiation but were afraid to ask. *Journal of Environmental Science and Health, Part C*, *39*(2), 113–128.

Chatterjee, A., & Schaefer, H. J. (1976). Microdosimetric structure of heavy ion tracks in tissue. *Radiation and Environmental Biophysics*, *13*(3), 215–227.

Elsässer, T., Cunrath, R., Krämer, M., & Scholz, M. (2008). Impact of track structure calculations on biological treatment planning in ion radiotherapy. *New Journal of Physics*, *10*(7), 075005.

Furusawa, Y., Fukutsu, K., Aoki, M., Itsukaichi, H., Eguchi-Kasai, K., Ohara, H., Yatagai, F., Kanai, T., & Ando, K. (2000). Inactivation of Aerobic and Hypoxic Cells from Three Different Cell Lines by Accelerated ^{3}He-, ^{12}C- and ^{20}Ne-Ion Beams. *Radiation Research*, *154*(5), 485–496.

Guo, Z., Zhou, G., & Hu, W. (2022). Carcinogenesis induced by space radiation: A systematic review. *Neoplasia*, *32*, 100828.

Han, Z.-B., Suzuki, H., Suzuki, F., Suzuki, M., Furusawa, Y., Kato, T., & Ikenaga, M. (1998). Relative Biological Effectiveness of Accelerated Heavy Ions for Induction of Morphological Transformation in Syrian Hamster Embryo Cells. *Journal of Radiation Research*, *39*, 193–201.

Hassler, D. M., Zeitlin, C., Wimmer-Schweingruber, R. F., Ehresmann, B., Rafkin, S., Eigenbrode, J. L., Brinza, D. E., Weigle, G., Böttcher, S., Böhm, E., Burmeister, S., Guo, J., Köhler, J., Martin, C., Reitz, G., Cucinotta, F. A., Kim, M.-H., Grinspoon, D., Bullock, M. A., ... Moores, J. E. (2014). Mars'

Surface Radiation Environment Measured with the Mars Science Laboratory's Curiosity Rover. *Science*, *343*(6169), 1244797.

Hawkins, R. B. (1996). A microdosimetric-kinetic model of cell death from exposure to ionizing radiation of any LET, with experimental and clinical applications. *International Journal of Radiation Biology*, *69*(6), 739–755.

Hawkins, R. B. (1994). A Statistical Theory of Cell Killing by Radiation of Varying Linear Energy Transfer. *Radiation Research*, *140*(3), 366–374.

Hawkins, R. B. (1998). A microdosimetric-kinetic theory of the dependence of the RBE for cell death on LET. *Medical Physics*, *25*(7), 1157–1170.

Hawkins, R. B. (2003). A Microdosimetric-Kinetic Model for the Effect of Non-Poisson Distribution of Lethal Lesions on the Variation of RBE with LET. *Radiation Research*, *160*(1), 61–69.

Kase, Y., Kanai, T., Matsufuji, N., Furusawa, Y., Elsässer, T., & Scholz, M. (2008). Biophysical calculation of cell survival probabilities using amorphous track structure models for heavy-ion irradiation. *Physics in medicine & biology*, *53*(1), 37–59.

Kiefer, J., & Straaten, H. (1986). A model of ion track structure based on classical collision dynamics (radiobiology application). *Physics in Medicine and Biology*, *31*(11), 1201–1209.

Lario, D., Decker, R. B., & Armstrong, T. P. (2001). Major solar proton events observed by IMP-8 (from 1973 to present). *Proceedings of ICRC 2001*, 3254.

López, M., & Martín, M. (2011). Medical management of the acute radiation syndrome. *Reports of Practical Oncology & Radiotherapy*, *16*(4), 138–146.

Mahaffy, P. R., Webster, C. R., Atreya, S. K., Franz, H., Wong, M., Conrad, P. G., Harpold, D., Jones, J. J., Leshin, L. A., Manning, H., Owen, T., Pepin, R. O., Squyres, S., Trainer, M., MSL Science Team, Kemppinen, O., Bridges, N., Johnson, J. R., Minitti, M., ... Moores, J. E. (2013). Abundance and Isotopic Composition of Gases in the Martian Atmosphere from the Curiosity Rover. *Science*, *341*(6143), 263–266.

Manganaro, L., Russo, G., Bourhaleb, F., Fausti, F., Giordanengo, S., Monaco, V., Sacchi, R., Vignati, A., Cirio, R., & Attili, A. (2018). 'Survival': A simulation toolkit introducing a modular approach for radiobiological evaluations in ion beam therapy. *Physics in Medicine & Biology*, *63*(8), 08NT01.

Manganaro, L., Russo, G., Cirio, R., Dalmasso, F., Giordanengo, S., Monaco, V., Muraro, S., Sacchi, R., Vignati, A., & Attili, A. (2017). A Monte Carlo approach to the microdosimetric kinetic model to account for dose rate time structure effects in ion beam therapy with application in treatment planning simulations. *Medical Physics*, *44*(4), 1577–1589.

Mangold, N., Baratoux, D., Witasse, O., Encrenaz, T., & Sotin, C. (2016). Mars: A small terrestrial planet. *The Astronomy and Astrophysics Review*, *24*(1), 15.

McMahon, S. J. (2018). The linear quadratic model: Usage, interpretation and challenges. *Physics in Medicine & Biology*, *64*(1), 01TR01.

Miller, R. C., Marino, S. A., Brenner, D. J., Martin, S. G., Richards, M., Randers-Pehrson, G., & Hall, E. J. (1995). The Biological Effectiveness of Radon-

Progeny Alpha Particles. II. Oncogenic Transformation as a Function of Linear Energy Transfer. *Radiation Research*, *142*, 54–60.

NASA. (2023). NASA Spaceflight Human-System Standard Volume 1, Crew Health. *NASA-STD-3001, Volume 1, Revision C*.

NCRP. (1988). Guidance on Radiation Received in Space Activities. NCRP Report No. 98 Bethesda. *NCRP Report No. 98. National Council on Radiation Protection and Measurements*.

NCRP. (2006). Information Needed to Make Radiation Protection Recommendations for Space Missions Beyond Low-Earth Orbit. *NCRP Report No. 153. National Council on Radiation Protection and Measurements*.

Ortiz, A. R., Rygalov, V. Y., & de León, P. (2015). Radiation Protection Strategy Development for Mars Surface Exploration. *45th International Conference on Environmental Systems*.

Prasanna, A., Ahmed, M. M., Mohiuddin, M., & Coleman, C. N. (2014). Exploiting sensitization windows of opportunity in hyper and hypo- fractionated radiation therapy. *Journal of Thoracic Disease*, *6*(4), 287–302.

Rahmanifard, F., De Wet, W. C., Schwadron, N. A., Owens, M. J., Jordan, A. P., Wilson, J. K., Joyce, C. J., Spence, H. E., Smith, C. W., & Townsend, L. W. (2020). Galactic Cosmic Radiation in the Interplanetary Space Through a Modern Secular Minimum. *Space Weather*, *18*(9), e2019SW002428.

Reames, D. V. (2023). Review and outlook of solar energetic particle measurements on multispacecraft missions. *Frontiers in Astronomy and Space Sciences*, *10*, 1254266.

Reznikoff, C. A., Bertram, J. S., Brankow, D. W., & Heidelberger, C. (1973). Quantitative and Qualitative Studies of Chemical Transformation of Cloned C3H Mouse Embryo Cells Sensitive to Postconfluence Inhibition of Cell Division. *Cancer Research*, *33*, 3239–3249.

Rohatgi, A. (2022). *WebPlotDigitizer* (Version 4.6).

Simpson, J. A. (1983). Elemental and Isotopic Composition of the Galactic Cosmic Rays. *Annual Review of Nuclear and Particle Science*, *33*(1), 323–382.

Singleterry, R. C., Blattnig, S. R., Clowdsley, M. S., Qualls, G. D., Sandridge, C. A., Simonsen, L. C., Norbury, J. W., Slaba, T. C., Walker, S. A., Badavi, F. F., Spangler, J. L., Aumann, A. R., Zapp, E. N., Rutledge, R. D., Lee, K. T., & Norman, R. B. (2010). OLTARIS: On-Line Tool for the Assessment of Radiation in Space. *NASA/TP–2010-216722*.

Townsend, L., Adams, J., Blattnig, S., Clowdsley, M., Fry, D., Jun, I., McLeod, C., Minow, J., Moore, D., Norbury, J., Norman, R., Reames, D., Schwadron, N., Semones, E., Singleterry, R., Slaba, T., Werneth, C., & Xapsos, M. (2018). Solar particle event storm shelter requirements for missions beyond low Earth orbit. *Life Sciences in Space Research*, *17*, 32–39.

Tylka, A. J., Dietrich, W., & Atwell, W. (2010–July 25). Band function representation of solar proton spectra in ground-level events. *38th Scientific Assembly of the Committee on Space Research (COSPAR)*.

Yang, T. C., Mei, M., George, K. A., & Craise, L. M. (1996). DNA damage and repair in oncogenic transformation by heavy ion radiation. *Advances in Space Research*, *18*, 149–158.

Yang, T. C., Craise, L. M., Mei, M.-T., & Tobias, C. A. (1985). Neoplastic Cell Transformation by Heavy Charged Particles. *Radiation Research*, *104*, S177–S187.

Appendix

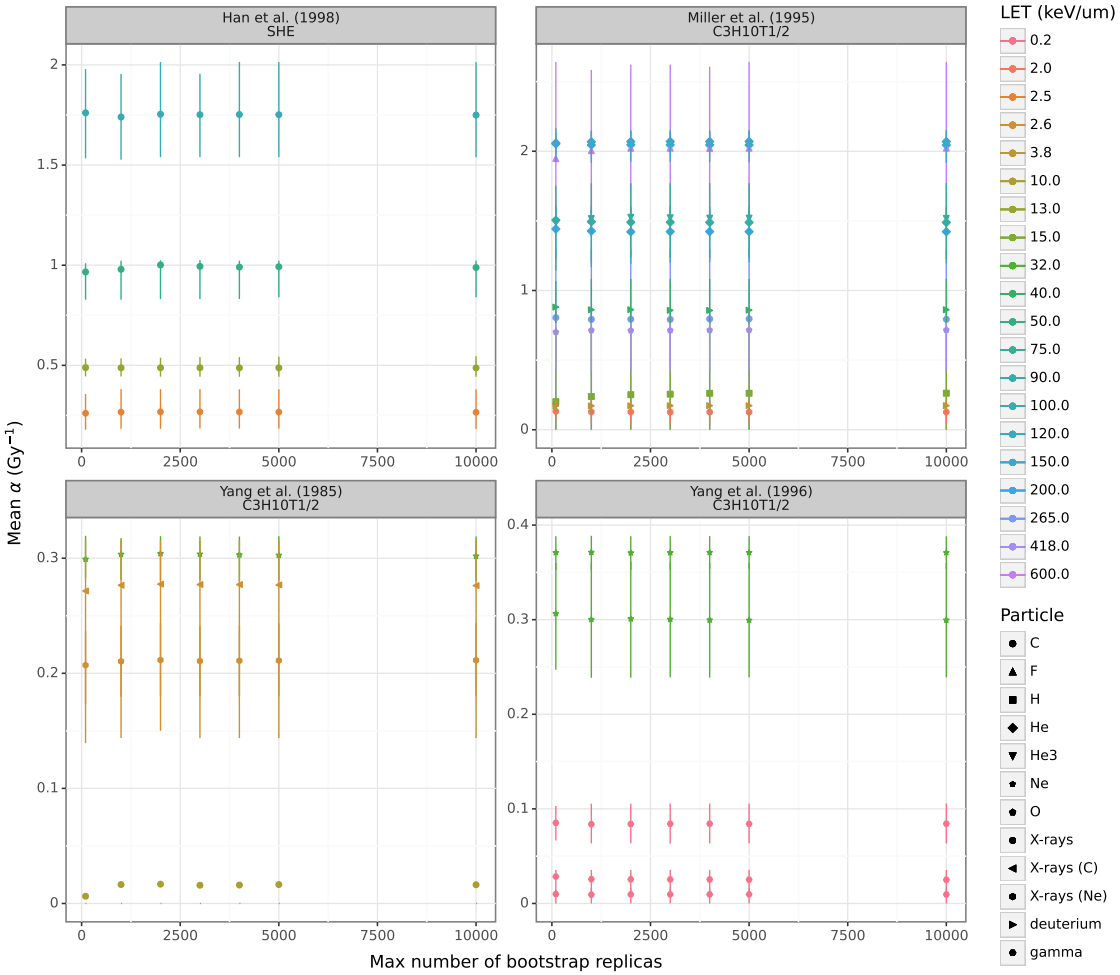

Figure 35. Mean α_S vs. maximum number of bootstrap replicas.

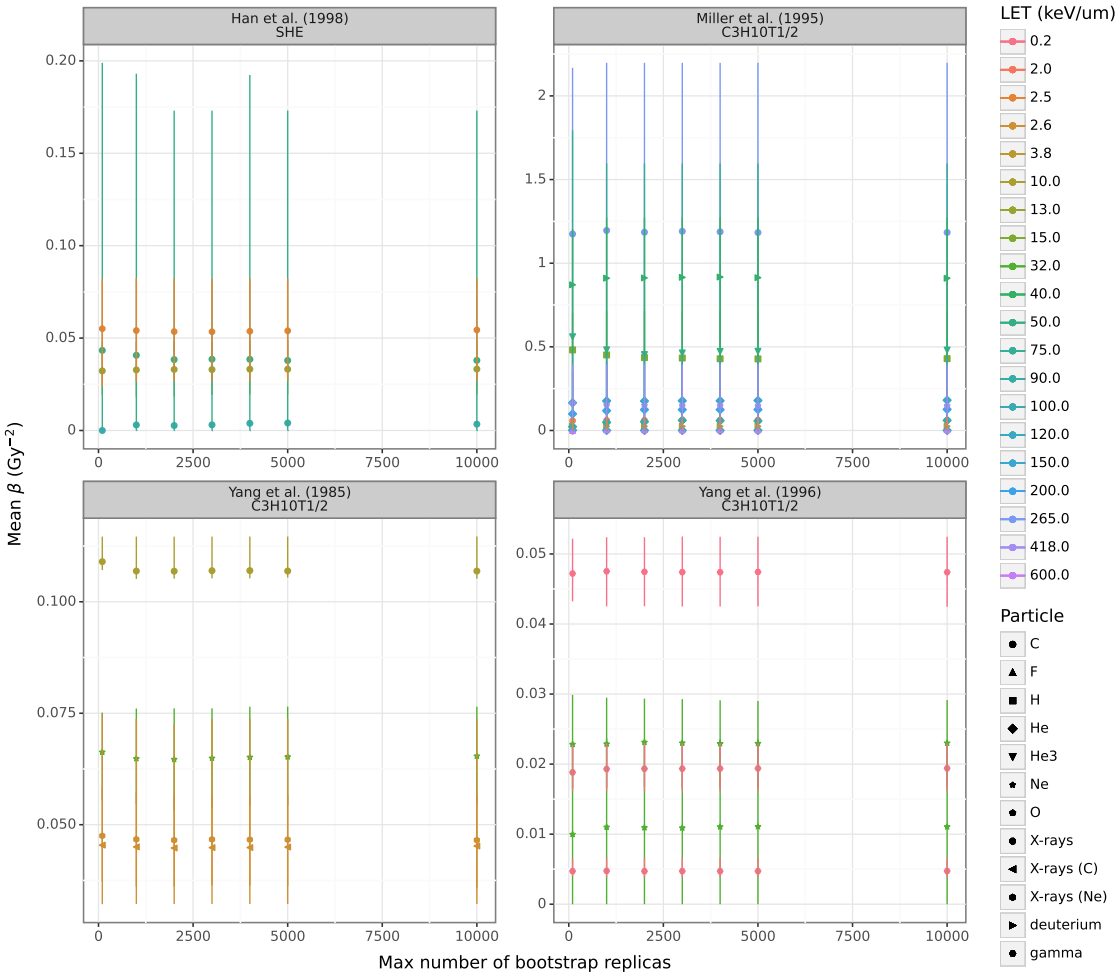

Figure 36. Mean β_S vs. maximum number of bootstrap replicas.

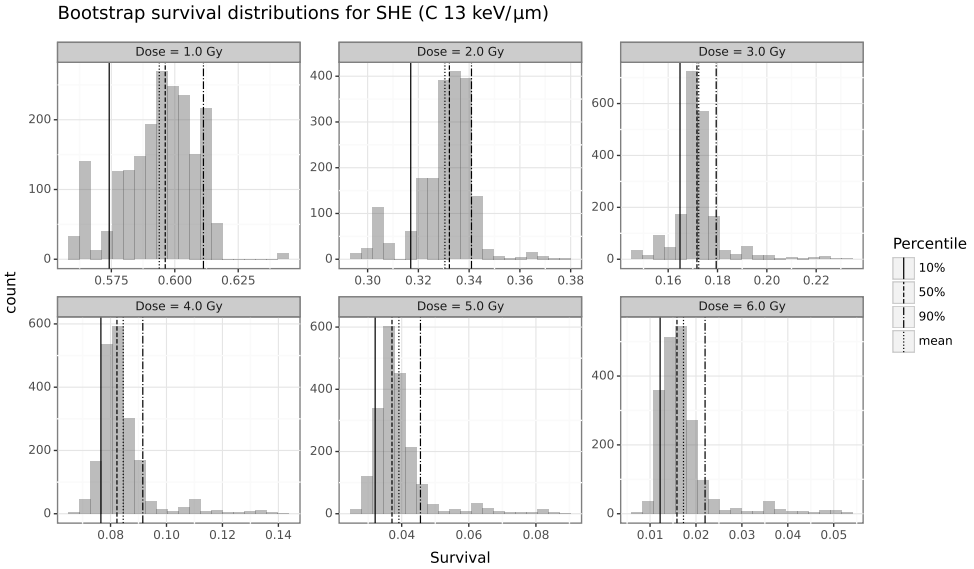

Figure 37. Bootstrap distributions of cell survival for different doses of 13 keV/μm carbon beams based on the Han et al. (1998) dataset.

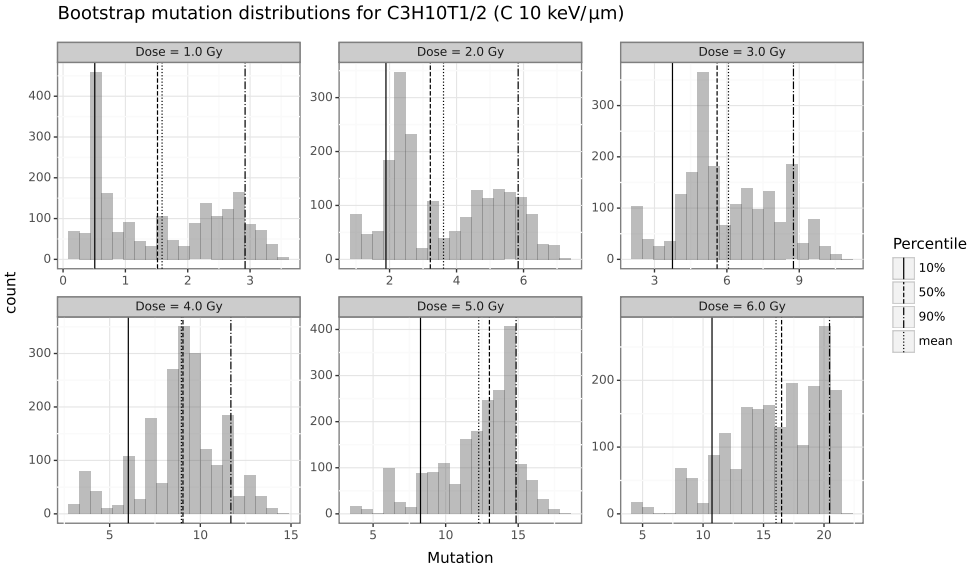

Figure 38. Bootstrap distributions of mutation for different doses of 10 keV/μm carbon beams based on the Yang et al. (1985) dataset.

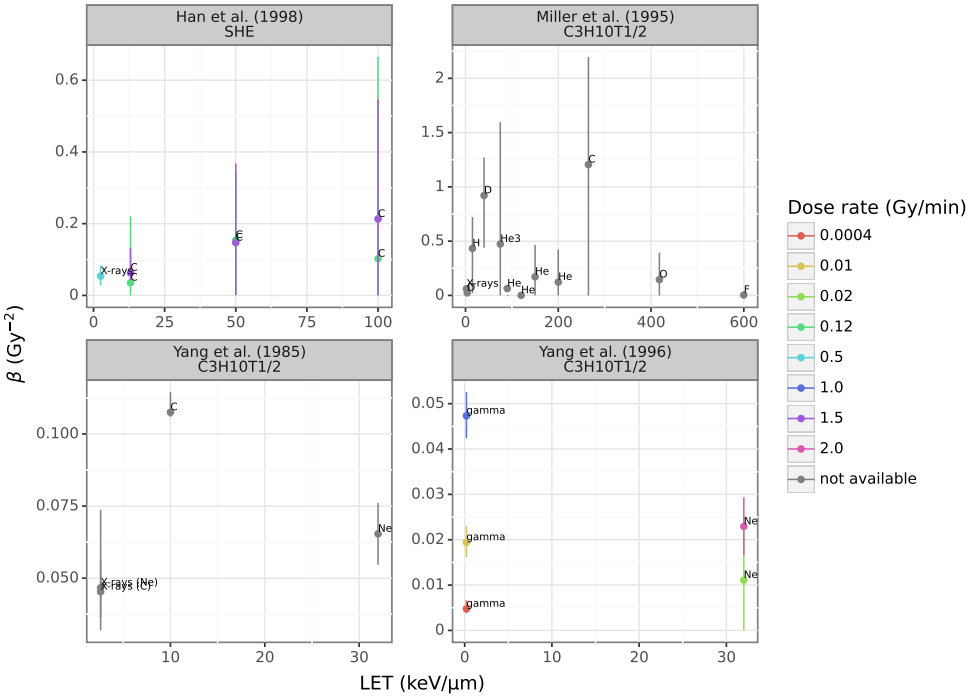

Figure 39. Experimental β vs. LET from survival data.

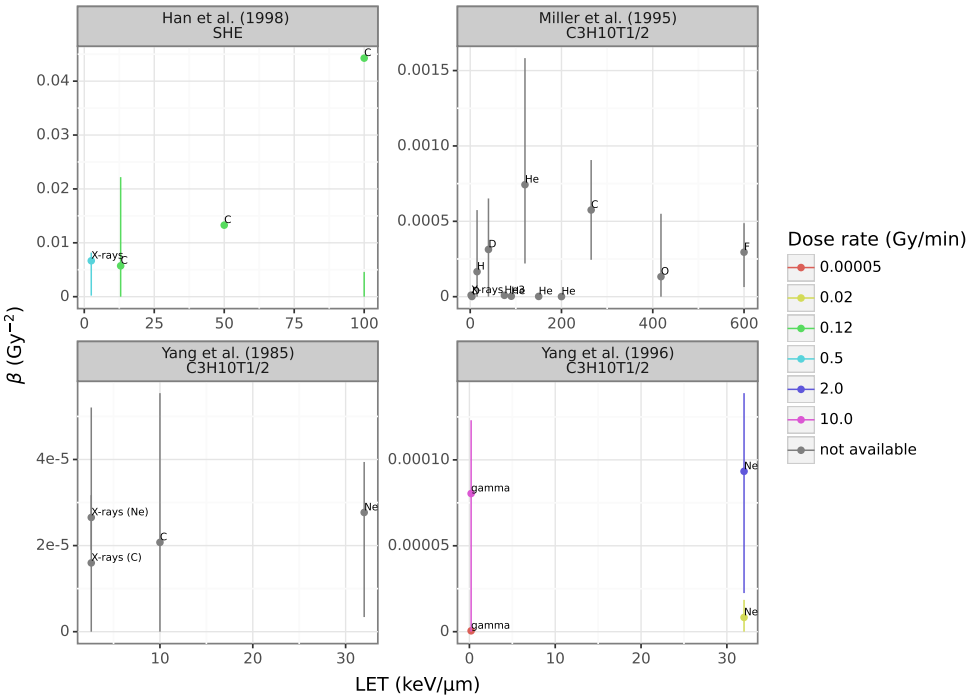

Figure 40. Experimental β vs. LET from mutation data.

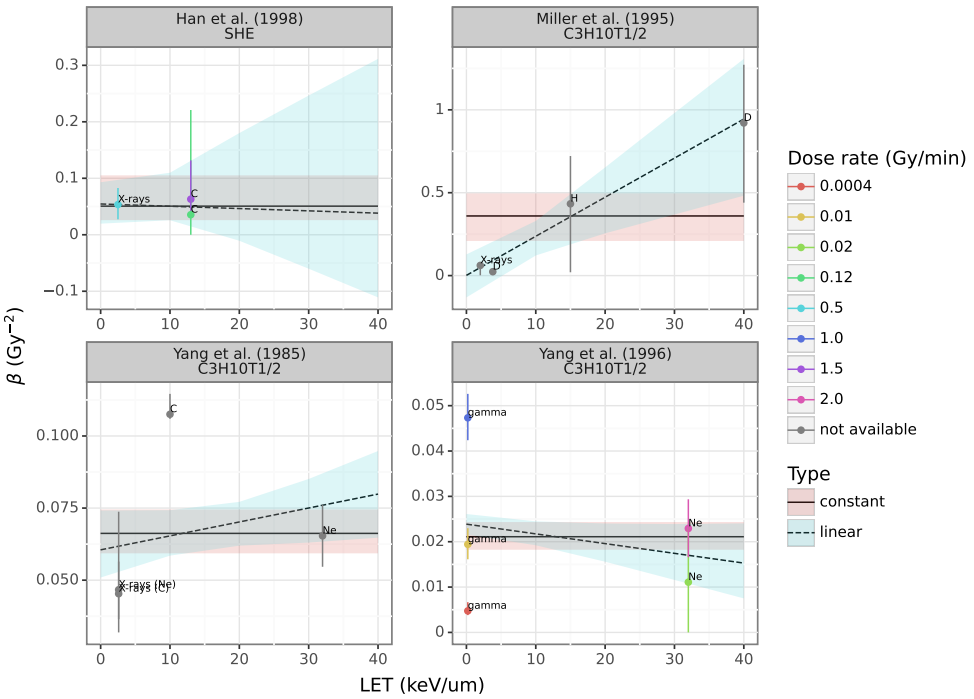

Figure 41. Linear fit of the mean of bootstrap β as a function of LET in survival data is shown with a dashed line. An average value of the mean of bootstrap β is shown with a solid line. Dose rates, when available, are indicated with colours.

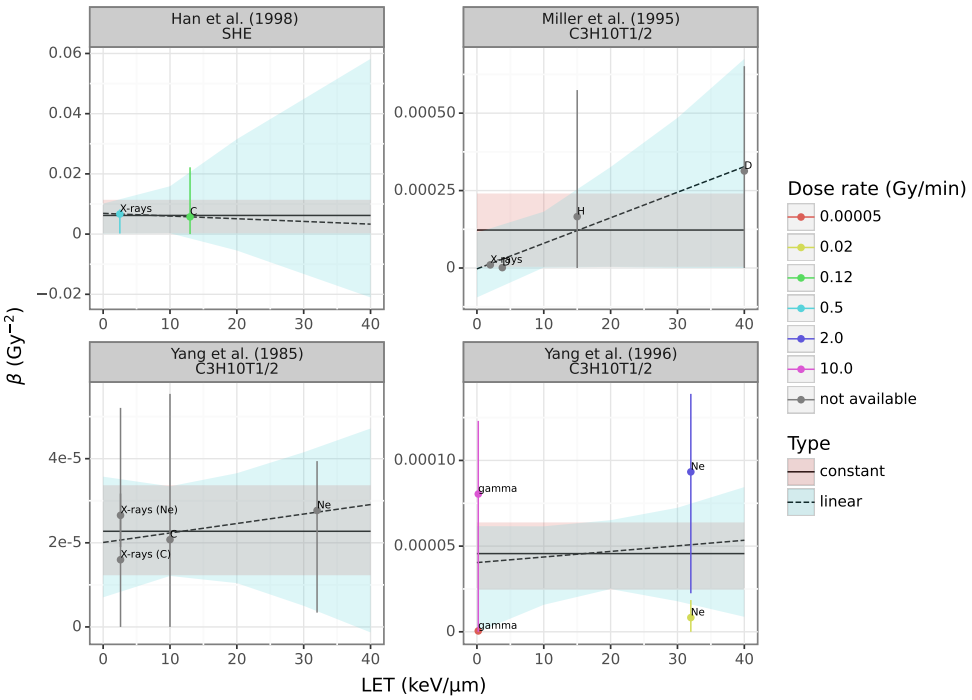

Figure 42. Linear fit of the mean of the bootstrap β as a function of LET in mutation data is shown with a dashed line. An average value of the mean of the bootstrap β is shown with a solid line. Dose rates, when available, are indicated with colours.

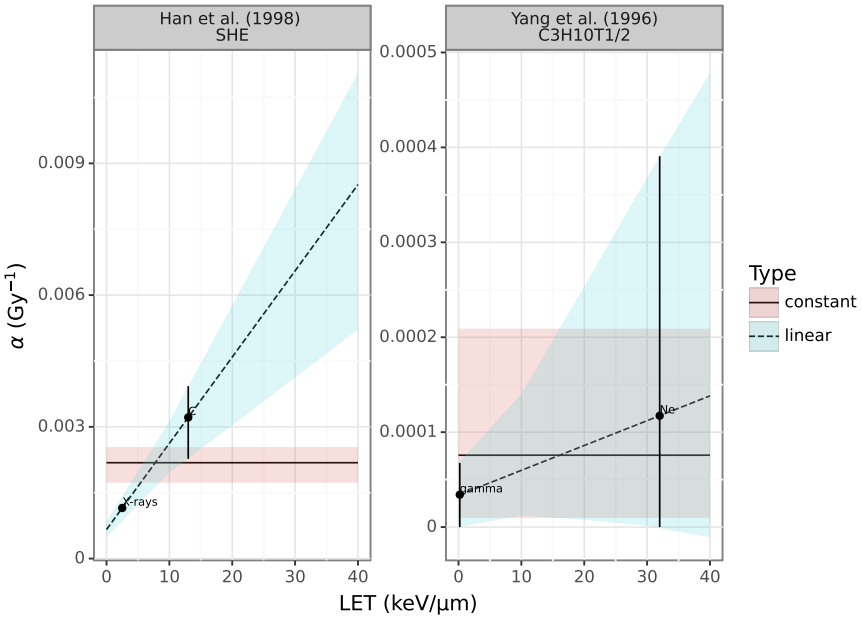

Figure 43. Linear fit of the mean of the bootstrap α as a function of LET in mutation data is shown with a dashed line, covering the simple linear fit line. An average value of the mean of bootstrap α is shown with a solid line.

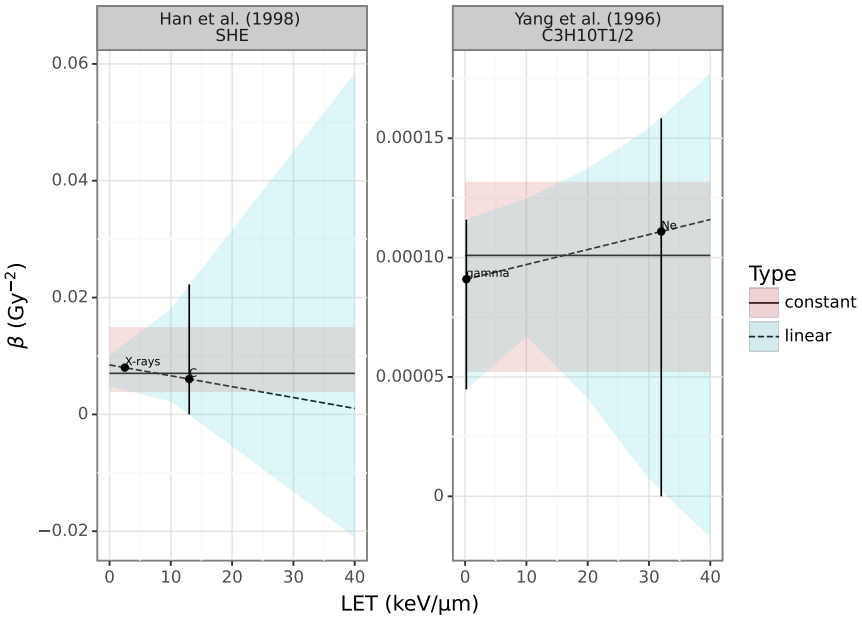

Figure 44. Linear fit of the mean of the bootstrap β as a function of LET in mutation data is shown with a dashed line, covering the simple linear fit line. An average value of the mean of bootstrap α is shown with a solid line.

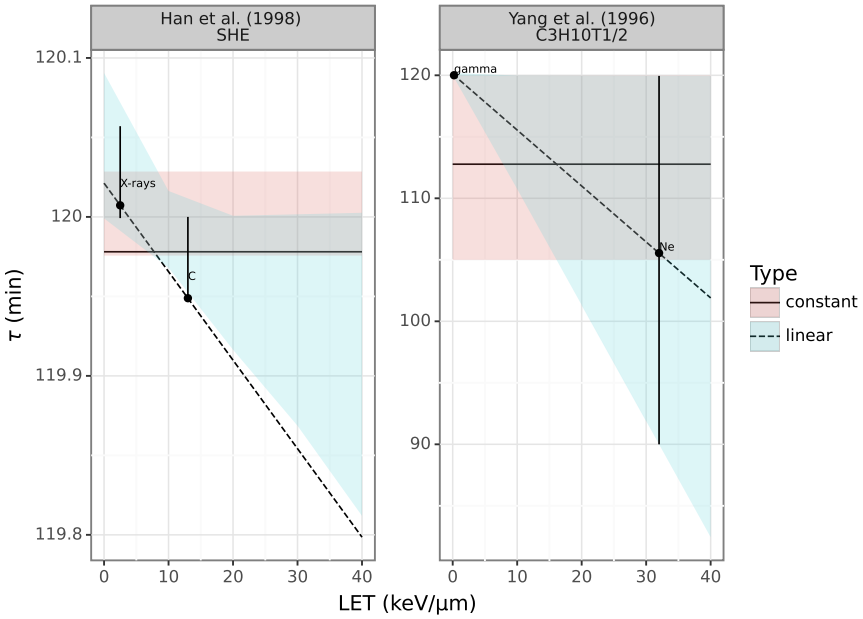

Figure 45. Linear fit of the mean of the bootstrap τ as a function of LET in mutation data is shown with a dashed line, covering the simple linear fit line. An average value of the mean of bootstrap τ is shown with a solid line.

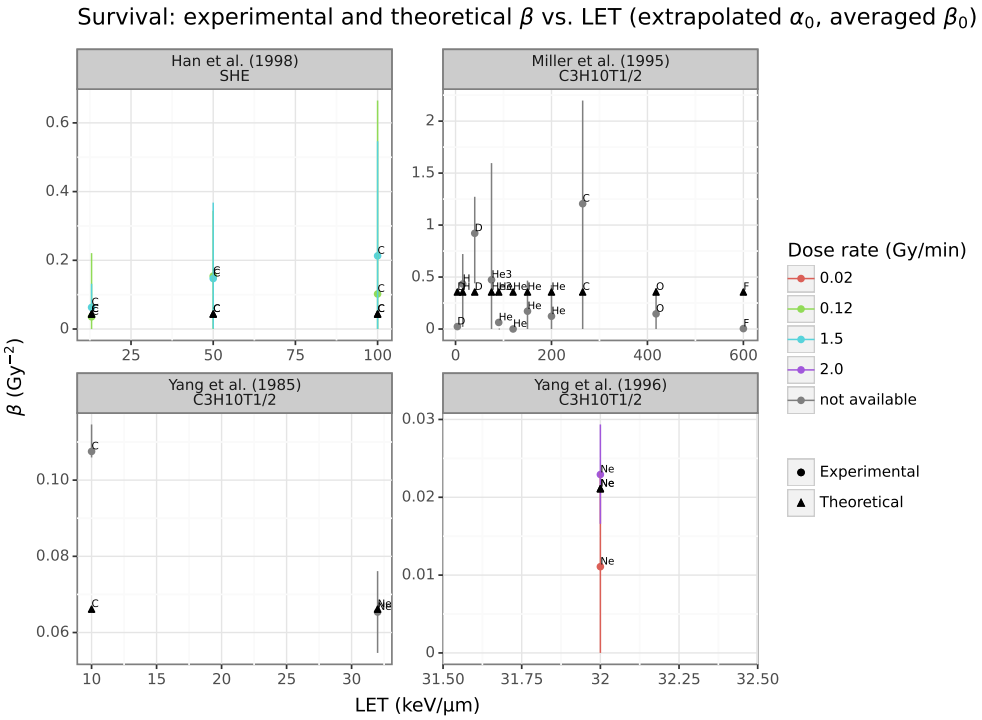

Figure 46. Experimental and theoretical values from the MKM simulation of β for survival are shown with different symbols. Parameters r_N and r_D in the MKM were optimised based on the linearly extrapolated α_0 and an average of β_0 of low LET ions. Dose rate was not included in the simulation as a parameter.

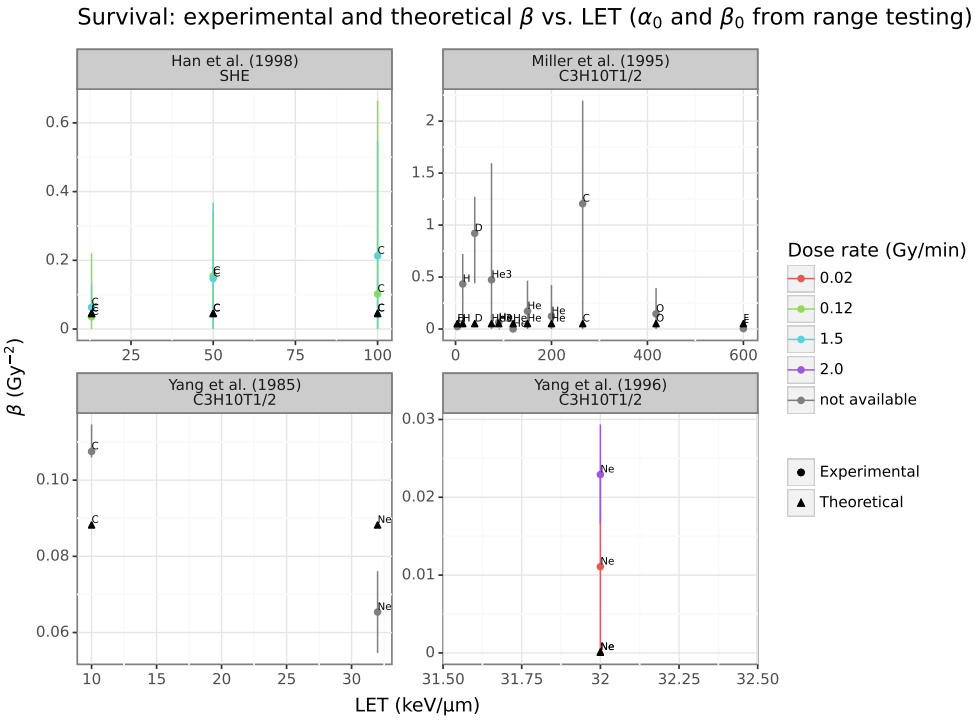

Figure 47. Experimental and theoretical values from the MKM simulation of β for survival are shown with different symbols. Parameters α_0, β_0, r_N and r_D in the MKM were optimised by testing a range of values and choosing the best fit to experimental data. Dose rate was not included in the simulation as a parameter.

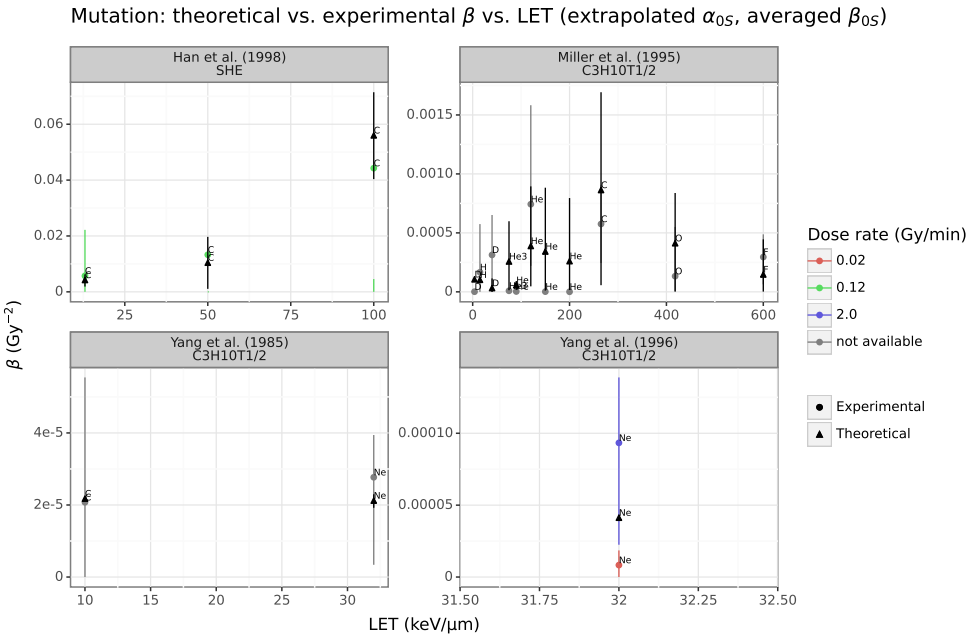

Figure 48. Experimental and theoretical values from the MKM simulation of β for mutation are shown with different symbols. Parameter r'_D in the MKM was optimised based on the linearly extrapolated α_0, linearly extrapolated α'_0, an average of β_0, and an average of β'_0 of low LET ions. Dose rate was not included in the simulation as a parameter.

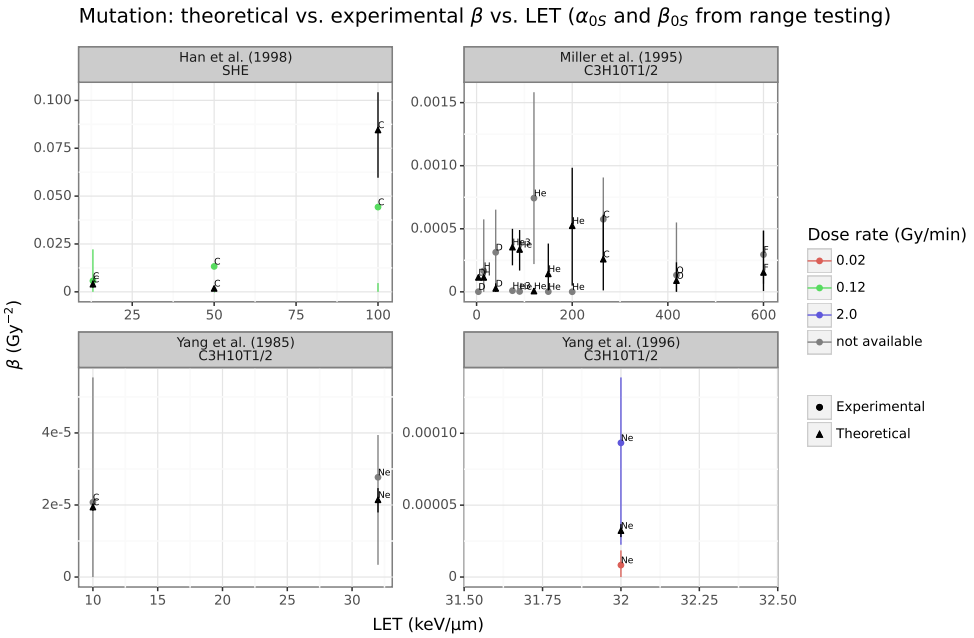

Figure 49. Experimental and theoretical values from the MKM simulation of β for mutation are shown with different symbols. Parameters α_0, β_0, r_N and r_D in the MKM were optimised by testing a range of values and choosing the best fit to experimental data, and the optimisation of the r'_D parameter was based on them. Dose rate was not included in the simulation as a parameter.

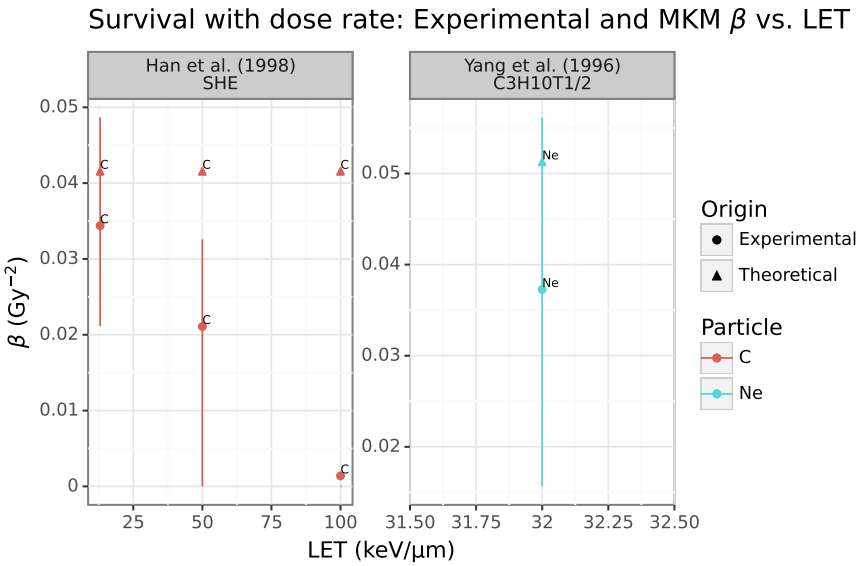

Figure 50. Experimental and theoretical values from the MKM simulation of β for survival are shown with different symbols. Parameters r_N and r_D in the MKM were optimised based on the linearly extrapolated α_0, an average of β_0, and an average of τ_0 of low LET ions.

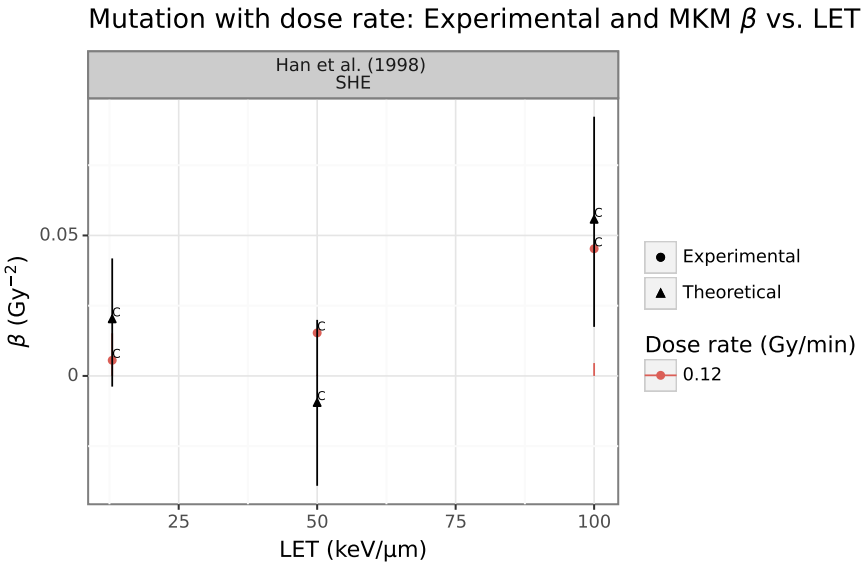

Figure 51. Experimental and theoretical values from the MKM simulation of β for mutation are shown with different symbols. Parameters r_N and r_D in the MKM were optimised based on the linearly extrapolated α_0, an average of β_0, and an average of τ_0 of low LET ions. Parameter r'_D was optimised based on the linearly extrapolated α_0, linearly extrapolated α'_0, an average of β_0, an average of β'_0, and an average of τ'_0 of low LET ions.

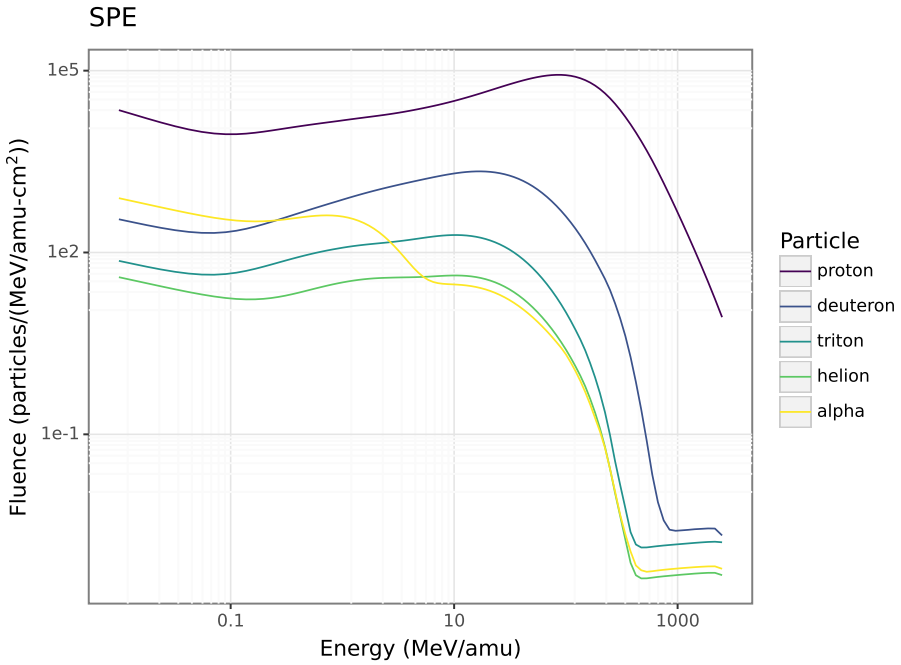

Figure 52. Fluence vs. energy for H and He as calculated during a solar particle event in Jezero crater on Mars.

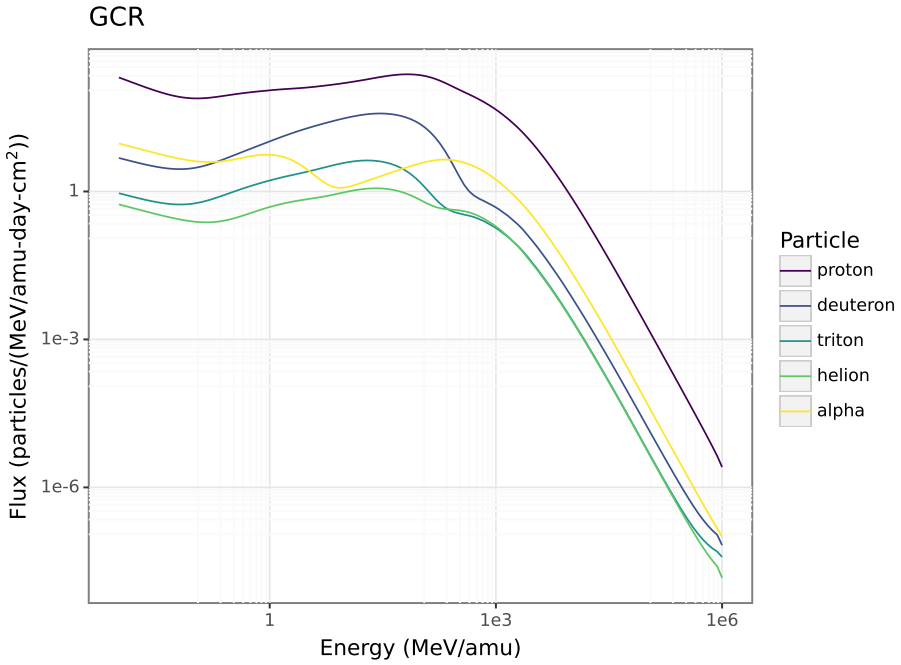

Figure 53. Flux vs. energy for H and He as calculated from galactic cosmic rays during a solar minimum in Jezero crater on Mars.